Chapter 2. Spatial Patterns of Speciated $PM_{2.5}$ Aerosol Mass Concentrations

Characterizing the contributions of major aerosol species to $PM_{2.5}$ gravimetric mass (mass of particles with aerodynamic diameters less than 2.5 μm) is essential for estimating visibility degradation, and analyzing the spatial variability of these species is critical for understanding their sources and local and regional impacts. Data from the IMPROVE network are particularly useful for these types of analyses, given the spatial distribution of sites and the long temporal record of the network. In addition to the mostly remote/rural sites operated by IMPROVE, the Environmental Protection Agency's (EPA) Chemical Speciation Network (CSN) collects $PM_{2.5}$ speciated aerosol data at approximately 150 urban/suburban monitoring sites. Data from the IMPROVE and CSN networks are useful independently, but by combining data from the two networks, a more complete spatial analysis of key aerosol species can be explored as a function of geographical region by specifically exploring the differences in urban and rural aerosol signatures. The 2016–2019 annual mean mass concentrations of ammonium sulfate (AS), ammonium nitrate (AN), particulate organic matter (POM), elemental carbon (EC), fine dust (FD), sea salt (SS), and $PM_{2.5}$ gravimetric fine mass (FM; $PM_{2.5}$ gravimetric mass and fine mass are used interchangeably in this report), reconstructed fine mass (RCFM, the sum of the above-listed major $PM_{2.5}$ aerosol species), and the fine mass residual (FM - RCFM) are examined. POM is calculated using organic carbon (OC) and an assumed organic carbon to organic mass ratio (OM/OC; POM = (OM/OC) × OC). Annual mean PM_{10} gravimetric mass (mass of particles with aerodynamic diameters less than 10 μm), and coarse mass (CM; the difference between PM_{10} and $PM_{2.5}$) are also presented in this chapter. PM_{10} measurements are not available at CSN sites, therefore data from the EPA PM_{10} FRM (Federal Reference Method) network were used (Hand et al., 2019a). Finally, the fractional contributions of major aerosol species to RCFM are presented.

Data aggregated over a 4-year period (2016–2019) are presented. To ensure that the data are representative of the entire period, completeness criteria were applied. Fifty percent completeness of the data (two years of valid monthly mean data) for a given site was required to be included in the analysis. Half of the total observations in a given month had to be valid for a monthly mean. In addition, 66% of each 3-month season was required for an annual mean (Debell et al., 2006; Hand et al., 2011). Seasons correspond to winter (December, January, February), spring (March, April, May), summer (June, July, August), and fall (September, October, November). These criteria were applied for each species separately. Data from the CSN were handled similarly. Values below the minimum detection limit (MDL) were handled according to how they were reported by each network, i.e., no additional substitutions were made for values below MDLs. Average reconstructed mass calculations were performed by summing the averages of individual species; for example, average concentrations of each species were computed and summed to obtain an average RCFM (Debell et al., 2006; Hand et al., 2011). Valid data for all of the species were required to compute monthly mean RCFM. This approach was used to avoid small sample sizes and provide a more accurate representation of average conditions. Applying the completeness criteria resulted in 153 IMPROVE sites and 136 CSN sites used in the analyses.

Annual mean concentration maps were created for each species from sites that met the completeness criteria. A Kriging algorithm was used to interpolate concentrations between site locations in order to create concentration isopleths (Isaaks and Mohan Srivastava, 1989). Maps

based on interpolation schemes should be viewed and interpreted with caution. The maps only are intended to help visualize the data and identify large spatial patterns. The density of site locations affects the interpolated fields, and neither the IMPROVE nor CSN networks have uniformly distributed site locations. Given these caveats, there is still interesting and useful information that can be gained from these maps, especially by examining the differences that occur when maps based only on the rural/remote IMPROVE sites are compared to those created when integrating the urban/suburban CSN and IMPROVE data. The following sections include discussions of spatial patterns for annual mean concentrations of AS, AN, POM, EC, FD, SS, FM, RCFM, the FM residual, PM_{10} mass, and CM. The top number in the scale shown on each contour map corresponds to the maximum concentrations for all sites; the contour levels themselves were created with the highest level corresponding to the 95th percentile in mass concentration and 5th and 95th percentile for the residual. Maps of species mass fractions are also included.

2.1 AEROSOL SPECIES COMPOSITION

Reconstructing $PM_{2.5}$ mass concentrations requires assumptions about the molecular form of assumed species. Table 2.1 presents the assumptions used in this report. More detail regarding each species will be presented in the following sections. Similar assumptions were made for IMPROVE and CSN unless otherwise noted in Table 2.1.

Table 2.1. Form of molecular species assumed in this report. Units in μg m^{-3} unless otherwise noted.

$PM_{2.5}$ Aerosol Species	**This Report**	**Assumptions**
Ammonium Sulfate (AS = $(NH_4)_2SO_4$)	1.375 × [SO_4^{2-}]	Sulfate [SO_4^{2-}] is assumed to be fully neutralized.
Ammonium Nitrate (AN = NH_4NO_3)	1.29 × [NO_3^-]	Nitrate [NO_3^-] is assumed to be ammonium nitrate.
Particulate Organic Matter (POM)	(OM/OC) × [OC]	OM/OC ratios account for additional species included in organic mass. A monthly-varying value was used for IMPROVE; seasonal-varying values were used for CSN (see below). OC is the sum of the subfractions from TOR analysis: OC = OC1 + OC2 + OC3 + OC4 + OP (see Section 1.2.2)
Elemental Carbon (EC)	EC	Also referred to as light absorbing carbon (LAC). EC is sum of subfractions from the TOR analysis: EC = EC1 + EC2 + EC3 – OP (see Section 1.2.2)
Filter light absorption (f_{abs})	f_{abs}	Hybrid integrating plate and sphere (HIPS) filter light absorption (Mm^{-1})
IMPROVE Fine Dust (FD)	1.15 × (2.2 × [Al] + 2.49 × [Si] + 1.63 × [Ca] + 2.42 × [Fe] + 1.94 × [Ti])	Soil potassium = 0.6 × [Fe]. Fe and Fe_2O_3 are equally abundant. A factor of 1.16 is used to account for other compounds such as MgO, Na_2O, H_2O and CO_3 (Malm et al., 1994). FD concentrations are multiplied by 1.15 based on multiple linear regression analyses (Hand et al., 2019b; see below).

$PM_{2.5}$ Aerosol Species	This Report	Assumptions
CSN Fine Dust (FD)	2.2 × [Al] + 2.49 × [Si] + 1.63 × [Ca] + 2.42 × [Fe] + 1.94 × [Ti]	Soil potassium = 0.6 × [Fe]. Fe and Fe_2O_3 are equally abundant. A factor of 1.16 is used to account for other compounds such as MgO, Na_2O, H_2O and CO_3.
Sea Salt (SS)	1.8 × [Cl^-]	Sea salt is 55% chloride ion by weight.
CSN Sea Salt (SS)	1.8 × [Cl]	Sea salt is derived using chlorine concentrations from XRF.
IMPROVE Gravimetric $PM_{2.5}$ Mass (FM)	$PM_{2.5}$	Mass of particles with aerodynamic diameters less than 2.5 μm.
CSN Gravimetric $PM_{2.5}$ Mass (FM)	$PM_{2.5}$	Mass of particles with aerodynamic diameters less than 2.5 μm using data from collocated EPA Federal Reference Method (FRM) network.
IMPROVE Gravimetric PM_{10} Mass	PM_{10}	Mass of particles with aerodynamic diameters less than 10 μm.
EPA PM_{10}	PM_{10}	Mass of particles with aerodynamic diameters less than 10 μm. Data from EPA's Federal Reference Method (FRM) network.
IMPROVE Coarse Mass (CM)	PM_{10} - $PM_{2.5}$	Difference in PM_{10} and $PM_{2.5}$.
EPA Coarse Mass (CM)	PM_{10} - $PM_{2.5}$	Difference in PM_{10} and $PM_{2.5}$ using collocated data from EPA's Federal Reference Method (FRM) network.
Reconstructed Fine Mass (RCFM)	AS + AN + POM + EC + FD + SS	Reconstructed fine mass algorithm represents $PM_{2.5}$ aerosol mass.
Fine Mass Residual	FM - RCFM	Difference in $PM_{2.5}$ gravimetric mass (FM) and reconstructed fine mass (RCFM).

Two changes from previous reports for estimating species mass include the calculation of POM and FD. Previous analyses of the fine mass residual identified increased biases over time that affected the agreement between gravimetric $PM_{2.5}$ mass and RCFM (Hand et al., 2019b). Results from a multilinear regression (MLR) analysis suggested that the constant OM/OC ratio of 1.8 that was previously applied in the RCFM algorithm was contributing to the bias. Applying a monthly varying value resulted in lower residuals and better agreement, especially in summer. The values applied are shown in Table 2.2. Seasonal values were assumed for the CSN based on Philip et al. (2014). IMPROVE FD concentrations were also determined to be low based on the MLR analysis and therefore were increased across the network and year by increasing the concentrations by 15%. A full discussion of these changes can be found in Appendix 2.1.

Table 2.2. OM/OC ratios used to calculate POM and applied in the reconstructed mass algorithm for the CSN and IMPROVE networks.

Month	IMPROVE	CSN
Jan	1.5	1.6
Feb	1.5	1.6
Mar	1.5	1.6
Apr	1.6	1.6
May	1.7	1.6
Jun	1.9	1.8

Month	IMPROVE	CSN
Jul	2.0	1.8
Aug	2.1	1.8
Sept	2.0	1.8
Oct	1.7	1.8
Nov	1.7	1.8
Dec	1.7	1.8

2.2 SPATIAL PATTERNS IN ANNUAL MEAN MASS CONCENTRATIONS

2.2.1 $PM_{2.5}$ Ammonium Sulfate Mass

The majority of sulfate in the atmosphere is produced through chemical reactions of sulfur dioxide (SO_2). Anthropogenic SO_2 is emitted through industrial activities such as coal and diesel fuel combustion. Regions that host electric utilities and industrial boilers (such as the eastern United States) are sources of SO_2 emissions that, combined with the elevated relative humidity or other aqueous pathways, create the most efficient conditions for sulfate production. The degree of acidity of sulfate (from acidic sulfuric acid to fully neutralized AS) depends on the availability of ammonia to neutralize the sulfuric acid formed from SO_2. Sulfate acidity can vary spatially and temporally (e.g., Lawal et al., 2018). In fact, recent studies have suggested that especially in the East, sulfate is in a more acidic form (Hidy et al., 2014; Kim et al., 2015; Lowenthal et al., 2015; Weber et al., 2016; Silvern et al., 2017; Lawal et al., 2018; Chen et al., 2019). However, without additional measurements of ammonium ion concentrations at IMPROVE sites, the degree of neutralization is unknown. A recent study suggests that potential biases associated with the assumed form of sulfate are relatively low (Hand et al., 2019b). These results are described in more detail in Appendix 2.1. For this report, sulfate is assumed to be in the form of fully neutralized AS (see Table 2.1), an upper bound of mass associated with dry sulfate.

The rural 2016–2019 IMPROVE annual mean AS concentrations ranged from 0.27 μg m^{-3} in White Pass, Washington (WHPA1), to 2.03 μg m^{-3} in Hawaii Volcanoes National Park (NP), Hawaii (HAVO1). The highest concentrations in the continental United States centered around the Ohio River valley and the Midsouth (1.5–2 μg m^{-3}) (see Figure 2.2.1a). The concentrations of AS decreased sharply toward the western United States, where concentrations were less than 1.0 μg m^{-3}, with the lowest concentrations at sites in the Northwest, Montana, and Idaho. Lower concentrations in the West reflected lower SO_2 emissions that lead to secondary particulate AS (Hand et al., 2020).

The regional nature of AS concentrations were evidenced by the similar concentrations of annual mean AS at the urban CSN sites (Figure 2.2.1b) and similar spatial variability in the two networks. A maximum annual mean CSN concentration of 3.23 μg m^{-3} occurred in southwestern Pennsylvania (Liberty, 420030064), somewhat higher than the maximum concentration observed in the IMPROVE network. The lowest concentration (0.37 μg m^{-3}) occurred at Butte, Montana (300930005). The addition of urban sites in the Ohio River valley, eastern Texas, and the Central Valley of California provided some additional structure in the isopleths in Figure 2.2.1b but did not alter the overall spatial pattern presented in Figure 2.2.1a.

AS contributed roughly a third of RCFM at rural sites in the eastern United States on an annual mean basis (see Figure 2.2.1c). Higher AS mass fractions (~0.30) stretched from sites in the Northeast, south toward western Texas. A transition to lower mass fractions occurred in the Intermountain West, with the lowest mass fractions occurring in the Northwest (<0.10). The highest IMPROVE AS mass fraction occurred in Hawaii Volcanoes NP (HAVO1, 0.70) where the highest AS annual mean concentrations occurred, most likely due to the high levels of volcanic emissions of SO_2. The lowest annual mean fraction occurred in Monture, Montana (MONT1, 0.06).

The spatial pattern of AS mass fraction for the combined rural and urban sites was similar to the rural-only distribution (Figure 2.2.1d), especially with respect to the large-scale spatial gradients. The highest urban fraction (0.37) also occurred in Hawaii (Kapolei, 150030010), although a much lower contribution than at the IMPROVE HAVO1 site. The lowest mass fraction (0.05) also occurred in Montana (Butte, 300930005). The combined urban and rural data demonstrated areas of relatively lower mass fractions in parts of the eastern United States, especially in the Southeast and Northeast, with fractions near 0.20. Other urban sites also had lower mass fractions, such as sites in the Front Range of Colorado; Salt Lake City, Utah; and Central Valley of California. Overall, the similarity in the urban and rural AS concentrations and fractions demonstrated the regional impact of the sources and atmospheric processes that lead to AS in the atmosphere.

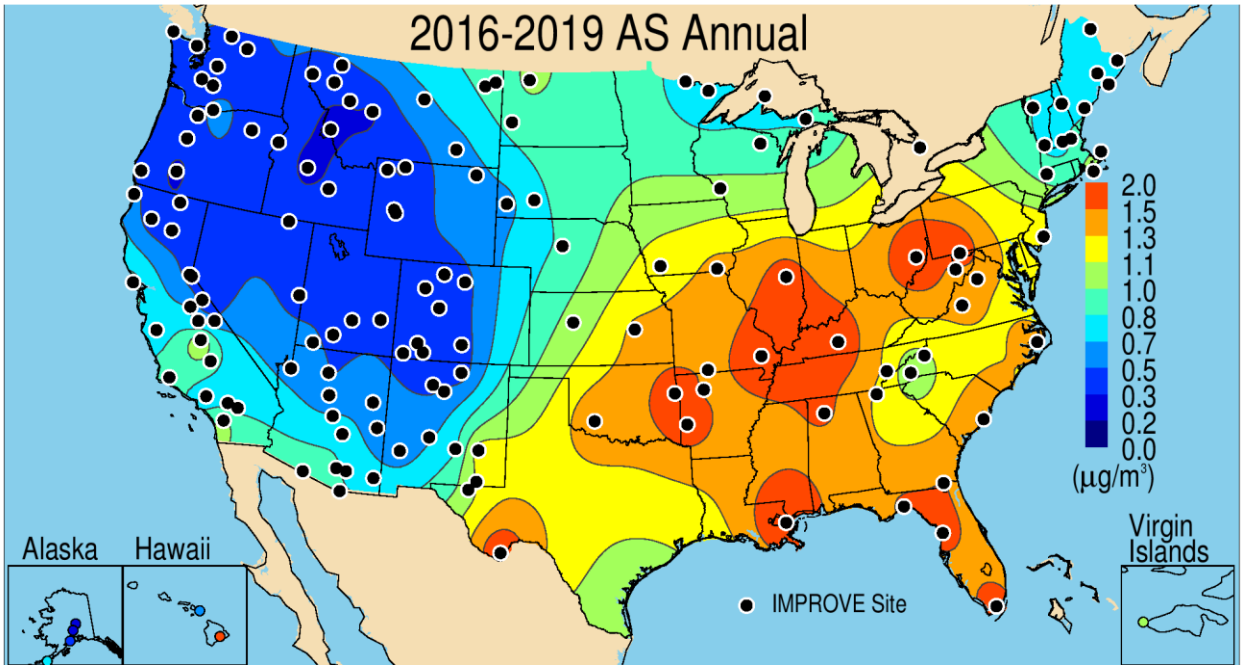

Figure 2.2.1a. IMPROVE 2016–2019 $PM_{2.5}$ ammonium sulfate (AS) annual mean mass concentrations (µg m^{-3}).

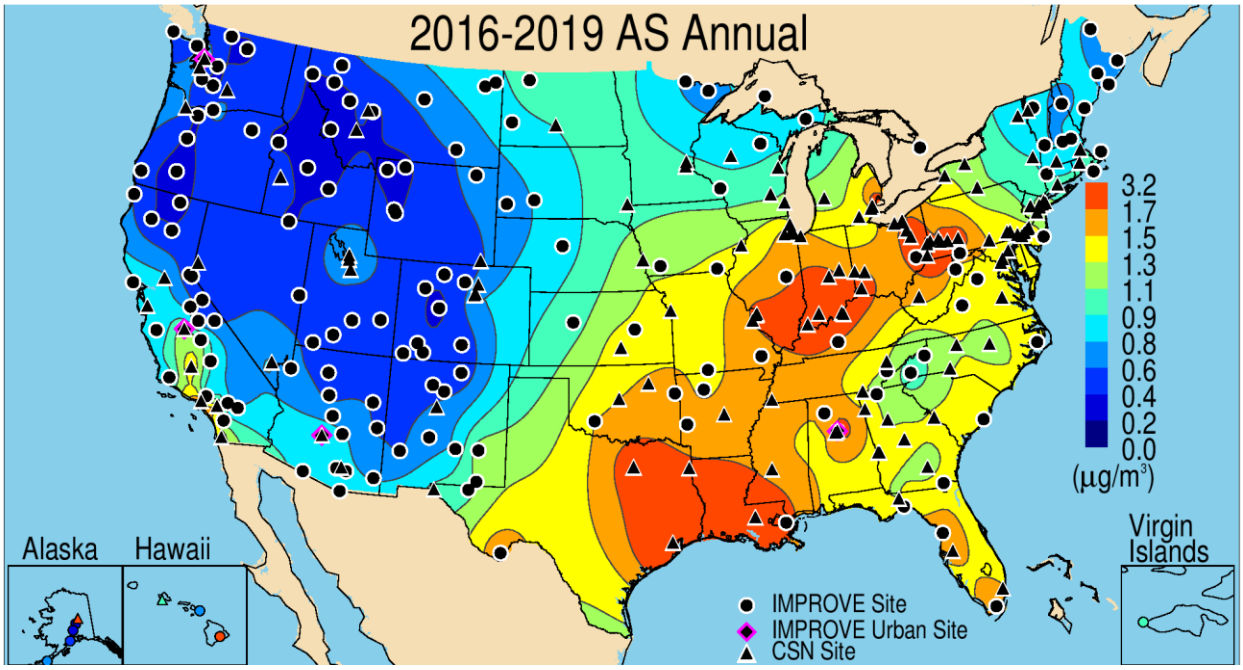

Figure 2.2.1b. IMPROVE and CSN 2016–2019 $PM_{2.5}$ ammonium sulfate (AS) annual mean mass concentrations (µg m^{-3}).

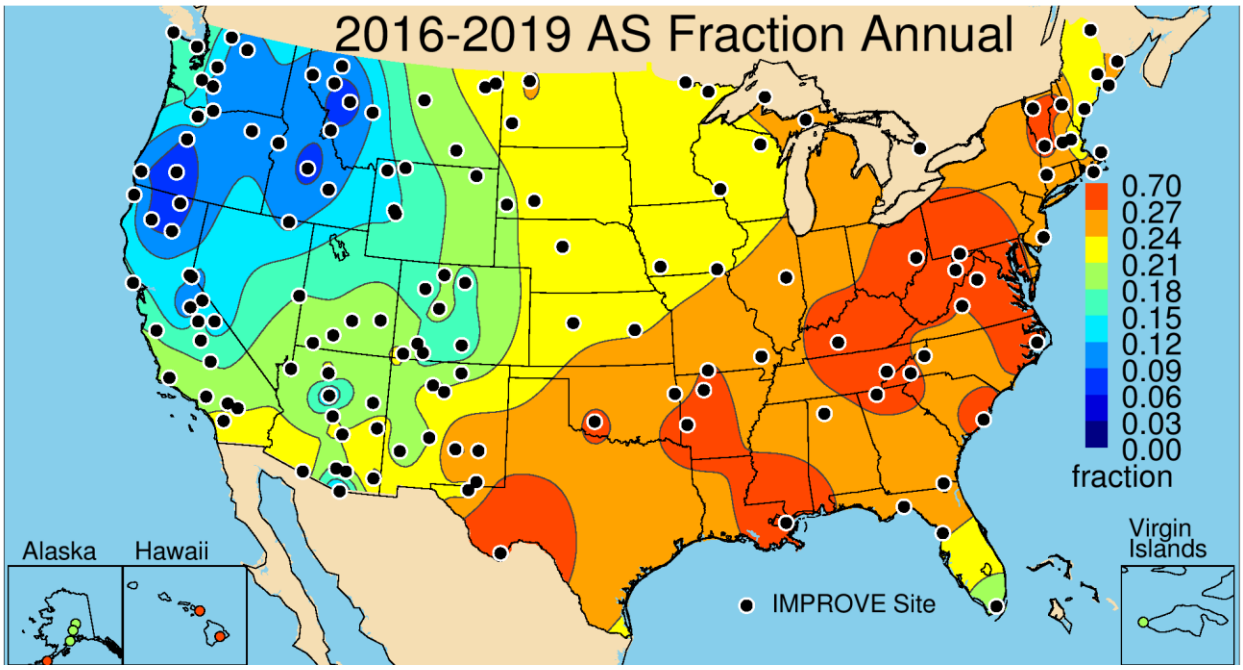

Figure 2.2.1c. IMPROVE 2016–2019 annual mean fraction contributions of ammonium sulfate (AS) to $PM_{2.5}$ reconstructed fine mass (RCFM).

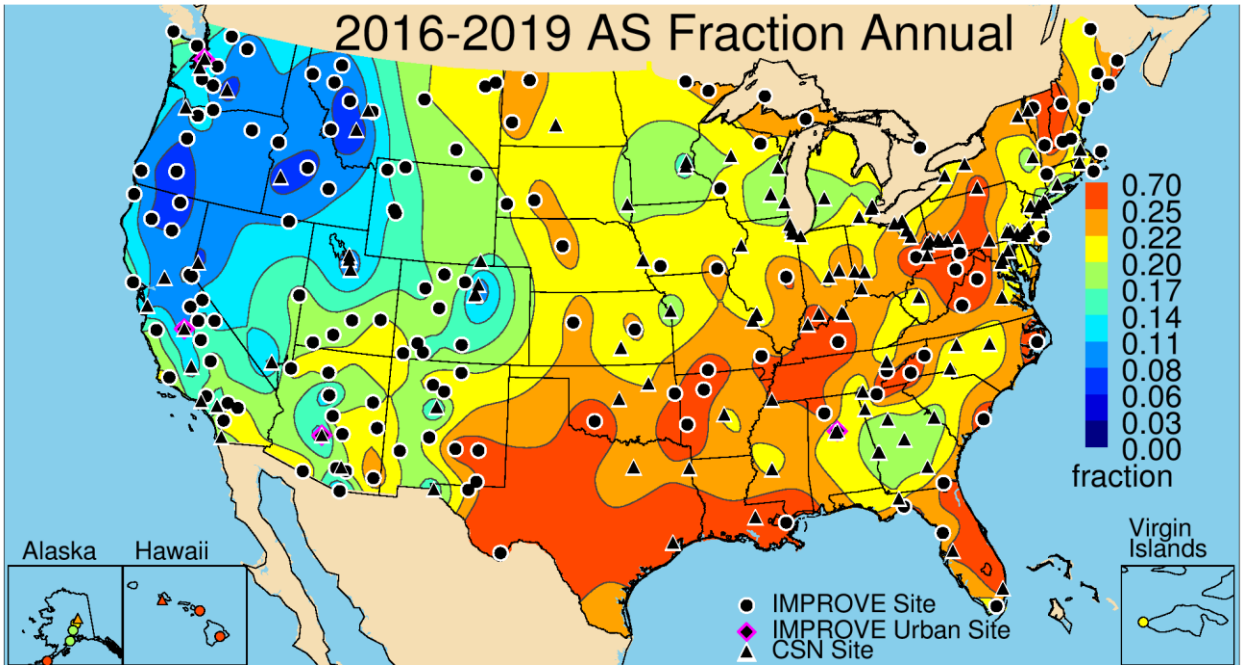

Figure 2.2.1d. IMPROVE and CSN 2016–2019 annual mean fraction contributions of ammonium sulfate (AS) to $PM_{2.5}$ reconstructed fine mass (RCFM).

2.2.2 $PM_{2.5}$ Ammonium Nitrate Mass

AN forms from the reversible reaction of gas-phase ammonia and nitric acid. Sources of oxidized nitrogen include combustion of fossil fuels from point sources such as coal-fired powered plants, on-road mobile sources, and non-road mobile sources. Other high-temperature processes such as biomass burning also contribute oxidized nitrogen, as do biogenic sources such as soil emissions (Vitousek et al., 1997). Sources of ammonia include agricultural activities, including animal husbandry, as well as mobile sources and natural emissions. The equilibrium reactions producing particle-phase AN are sensitive to small changes in temperature and relative humidity that can shift the equilibrium between the particle and gas phase. Lower temperatures and higher relative humidity favor particulate AN, while higher temperatures and lower relative humidity favor the gas phase. Nitrate (as AN) is often assumed to be in the fine mode, and this is probably a reasonable assumption in regions with high ammonia and nitric acid concentrations and low sulfate concentrations (Lee et al., 2008). The central United States is an area of high agricultural activity and is associated with high nitrate and ammonium concentrations that can lead to elevated fine-mode AN concentrations (Pitchford et al., 2009; Heald et al., 2012; Warner et al., 2017; Hu et al., 2020). Using data reported by Lee et al. (2008), Hand and Malm (2006) found that when fine-mode nitrate concentrations were greater than 0.5 μg m^{-3}, AN contributed over 70% of the observed total nitrate in the fine mode at certain locations. However, Lee et al. (2008) showed that in many locations nitrate is associated with the coarse mode from reactions of gas-phase nitric acid with sea salt or calcium carbonate. Allen et al. (2015) reported similar results during the 2013 Southern Oxidant and Aerosol Study in the Southeast, and Malm et al. (2007) reported regions and seasons with high nitrate concentrations in the coarse mode at a subset of IMPROVE sites. For the purposes of reconstructing fine mass and light extinction coefficients, and because the necessary measurements to determine the form of nitrate are not regularly available, nitrate is assumed to be in the form of AN.

The area of high annual mean AN concentrations in the central United States (Figure 2.2.2a) is associated with agricultural activity in the region. The maximum IMPROVE 2016–2019 rural AN annual mean concentration of 1.92 μg m^{-3} occurred at Bondville, Illinois (BOND1), a site located in the agricultural Midwest. Sites in central and southern California were also associated with higher AN concentrations, as were sites in northern North Dakota, with concentrations near 1.0 μg m^{-3}. High concentrations at sites in North Dakota may be associated with oil and gas energy development (Prenni et al., 2016; Evanoski-Cole et al., 2017; Gebhart et al., 2018). Concentrations were much lower outside of the central United States, especially at sites in the Intermountain West and Northwest, with concentrations less than 0.5 μg m^{-3}. Similarly low annual mean concentrations were observed in the Southeast and Northeast. The lowest rural concentration occurred in Denali NP, Alaska (0.05 μg m^{-3}, DENA1).

The inclusion of CSN sites provided more spatial resolution to the rural AN spatial pattern and showed the impact of urban AN concentrations on surrounding areas (Figure 2.2.2b). High AN was associated with sites surrounding Lake Michigan, and other hot spots occurred near Denver, Colorado and Salt Lake City, Utah. The highest urban annual mean AN concentration (4.5 μg m^{-3}) occurred at Bakersfield, California, (060290014) and other urban sites in the Central Valley. The lowest CSN AN concentration occurred at Kapolei, Hawaii (0.18 μg m^{-3}, 150030010). Generally, urban concentrations of AN were considerably higher than rural concentrations.

Sites with high contributions of AN to RCFM were similar to those with high annual mean AN concentrations. The central United States, northern North Dakota, and California sites are examples, with annual mean AN RCFM fractions near 0.25–0.30 (Figure 2.2.2c). The rural IMPROVE site at Great River Bluffs, Minnesota (GRRI1), had the highest annual contribution of AN to RCFM (0.31), compared to the lowest at Monture, Montana (0.02, MONT1). In general, most rural IMPROVE sites were not highly influenced by AN contributions to RCFM on an annual mean basis. Lower contributions (~0.05) of AN to RCFM occurred at sites in the Southeast and across the Intermountain West. With the addition of the urban CSN sites, the influence of the contribution of AN to RCFM extended farther west from the central United States (Figure 2.2.2d), where AN contributed over a quarter of RCFM at sites in Colorado and central California, and the maximum contribution occurred at Bountiful, Utah (0.34, 490110004). The lowest urban CSN fraction (0.04) occurred in the southern Georgia city of Douglas (130690002).

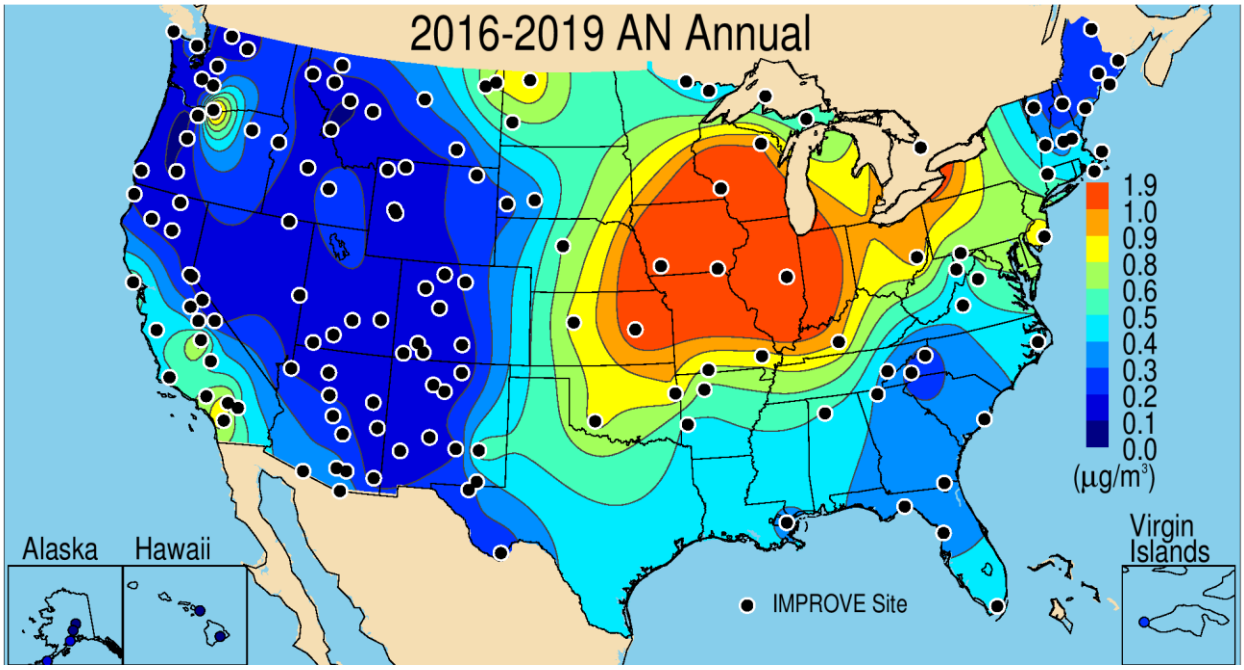

Figure 2.2.2a. IMPROVE 2016–2019 $PM_{2.5}$ ammonium nitrate (AN) annual mean mass concentrations (µg m^{-3}).

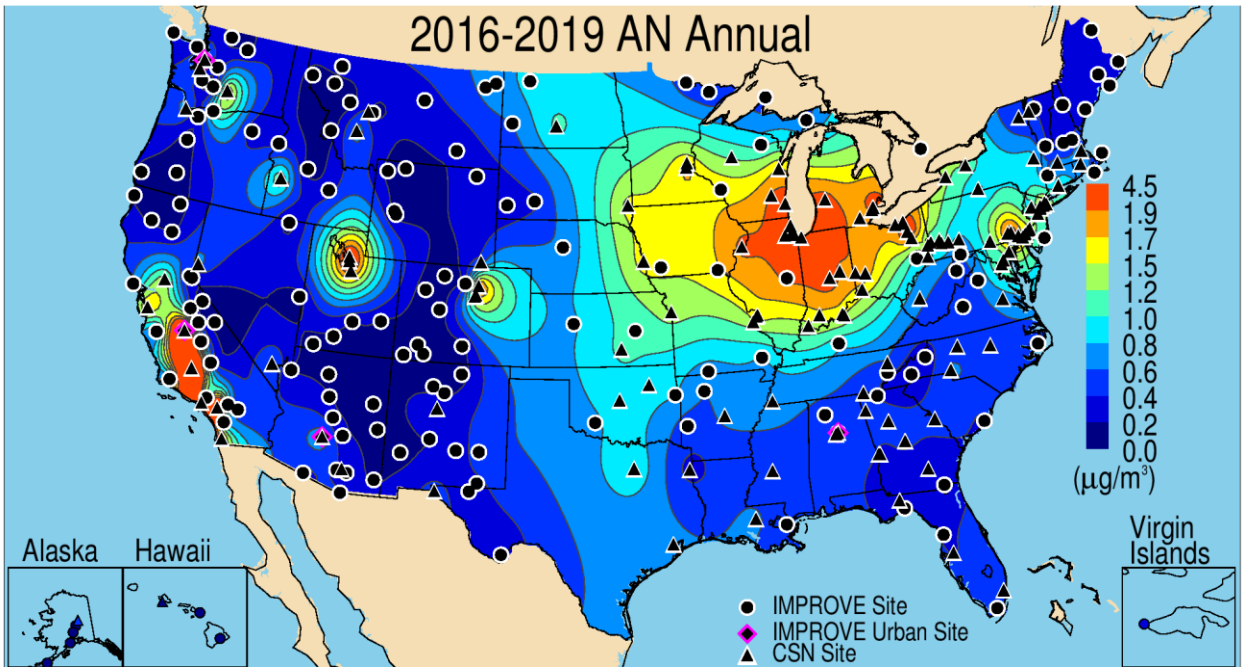

Figure 2.2.2b. IMPROVE and CSN 2016–2019 $PM_{2.5}$ ammonium nitrate (AN) annual mean mass concentrations (µg m^{-3}).

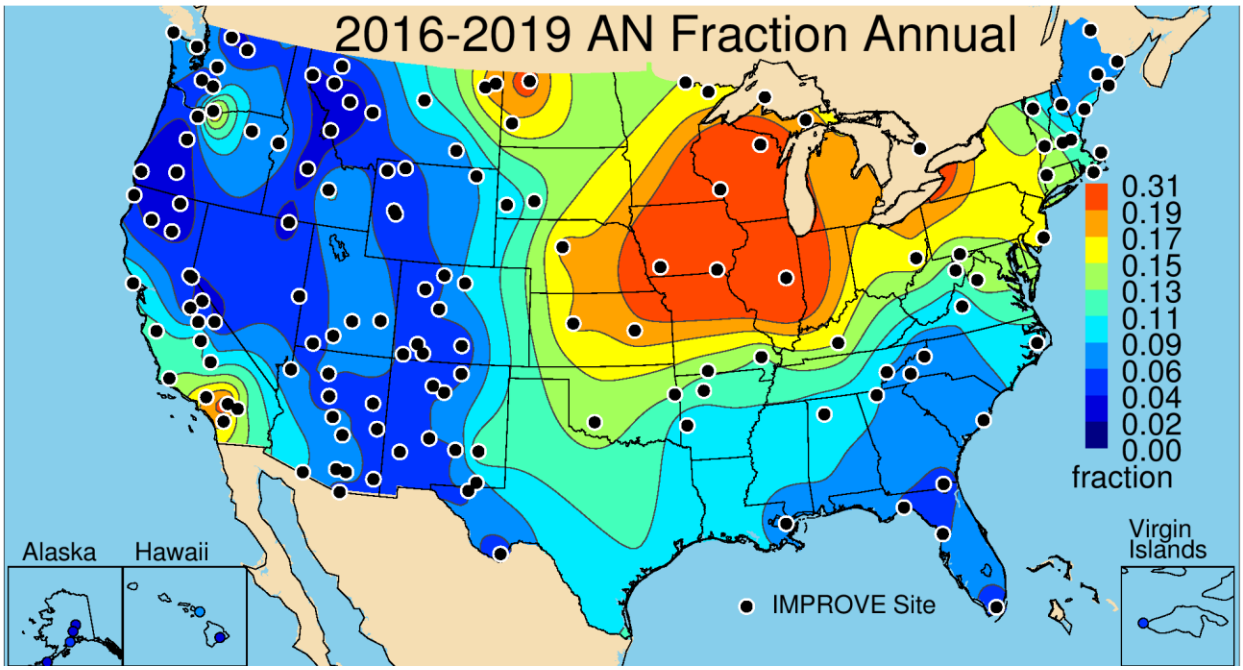

Figure 2.2.2c. IMPROVE 2016–2019 annual mean fraction contributions of ammonium nitrate (AN) to $PM_{2.5}$ reconstructed fine mass (RCFM).

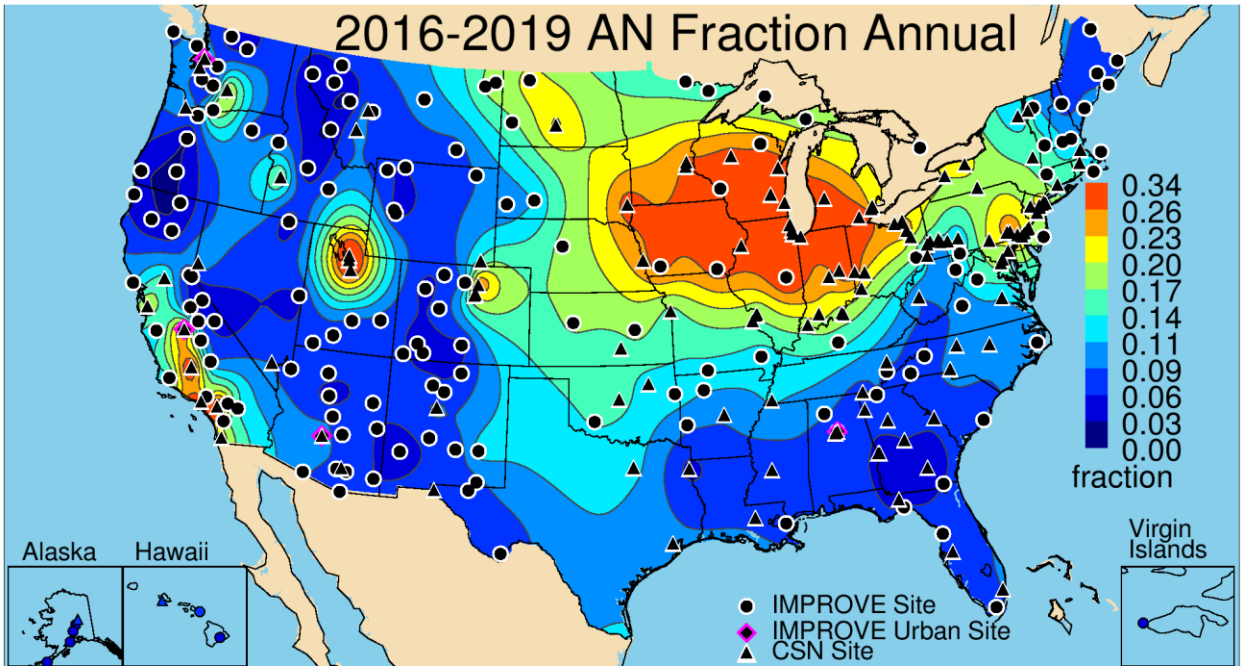

Figure 2.2.2d. IMPROVE and CSN 2016–2019 annual mean fractions of ammonium nitrate (AN) to $PM_{2.5}$ reconstructed fine mass (RCFM).

2.2.3 $PM_{2.5}$ Particulate Organic Matter Mass

The sources of POM in the atmosphere are both primary emissions and secondary formation. Primary emissions include particle mass emitted directly from combustion of fossil fuels or biomass. Secondary organic aerosol formation results from the oxidation of gas-phase precursors from both anthropogenic and biogenic sources. Accurate estimates of POM from OC

are required in order to compute RCFM and to estimate optical properties such as light scattering coefficients. The OM/OC ratio used to estimate POM takes into account contributions from other elements associated with the organic matter, such as nitrogen, oxygen, and hydrogen. It is spatially and temporally variable. Typical values range from 1.2 to 2.6. It is impossible to determine which and how many elements are associated with POM without knowing the chemical formula of the organic compound, and it is common for a significant portion of organic aerosol mass to remain unidentified (Turpin and Lim, 2001; Jimenez et al., 2009; Heald and Kroll, 2020). Because the organic compounds that compose POM are typically unknown, the approach for taking into account other elements in POM mass has been to apply an average OM/OC ratio. However, recent measurements and statistical studies have indicated the seasonal and regional variability in OM/OC. For example, values in warm months tend to be higher than cold months, and values in rural areas tend to be higher than in urban areas (e.g., Bae et al., 2006; Aiken et al., 2008; Polidori et al., 2008; El-Zanan et al., 2005; 2009; Lowenthal et al., 2009; Malm et al., 2011; Simon et al., 2011; Hallar et al., 2013; Philip et al., 2014; Ruthenburg et al., 2014; Lowenthal et al., 2015; Blanchard et al., 2016; Hand et al., 2019b; Malm et al., 2020). Following the methods in Hand et al. (2019b), a multiple linear regression was performed with monthly resolution using IMPROVE data from 2016 through 2019. Results suggested that the monthly variability in OM/OC ratios was consistent with other studies in rural areas, therefore these values were used to compute POM for the IMPROVE network (Table 2.2) to be more consistent with recent literature and to address issues related to biases in the fine mass residual (see Appendix 2.1). To compute POM using CSN data, estimates from Philip et al. (2014) were applied on a seasonal basis (Table 2.2).

The highest 2016–2019 annual mean rural IMPROVE POM concentrations occurred in southern Florida, the northwestern United States, and central and northern California due to the influence of biomass burning (Figure 2.2.3a). The highest concentrations occurred in Yosemite NP, California (6.8 $\mu g\ m^{-3}$, YOSE1). Elevated levels of POM (~3.0 $\mu g\ m^{-3}$) also occurred at sites in the Southeast, as well as at sites in the Northwest and California. The 2016–2019 period was associated with high fire activity, especially 2017 and 2018 in the Northwest, and 2016 in the Southeast. The lowest annual mean concentrations occurred in Haleakala Crater NP, Hawaii (0.15 $\mu g\ m^{-3}$, HACR1). Annual mean concentrations in western Colorado, portions of Wyoming and New Mexico, and the Four Corners region were less than 1 $\mu g\ m^{-3}$.

The combined urban and rural POM concentrations demonstrated the influence of urban POM sources, with higher concentrations at sites in the Southeast and along the Central Valley of California (Figure 2.2.3b). Sites in Alabama, Georgia, South Carolina, and North Carolina had POM concentrations greater than 4.0 $\mu g\ m^{-3}$. The highest annual mean CSN POM concentration occurred at Fresno, California (6.01 $\mu g\ m^{-3}$, 060190011). Similar maximum annual mean rural and urban POM concentrations demonstrated the influence of biomass burning on rural POM concentrations. As in the IMPROVE network, the lowest annual mean CSN POM concentration occurred in Hawaii (0.42 $\mu g\ m^{-3}$, Kapolei, 150030010).

The IMPROVE sites with the highest contributions (>0.7) of POM to RCFM occurred in the northwestern United States, in regions influenced by biomass smoke emissions (see Figure 2.2.3c). The highest fraction occurred in Crater Lake NP, Oregon (0.79, CRLA1). At sites cross most of the United States, annual mean POM fractions were around 0.5, with somewhat higher fractions (0.55–0.60) occurring at sites in the Southeast and Northeast. The lowest rural fractions

in the continental United States occurred in the Southwest, and the lowest fraction of all rural sites occurred in Hawaii Volcanoes NP, Hawaii (0.09, HAVO1). The general spatial pattern did not change with the addition of CSN sites (Figure 2.2.3d), with higher contributions at sites in the Northwest. The highest CSN annual mean POM fraction (0.65) occurred at Butte, Montana (300930005). Similar to rural sites, urban POM fractions were generally high at sites in the Southeast, including several urban sites in Georgia with fractions greater than 0.65.

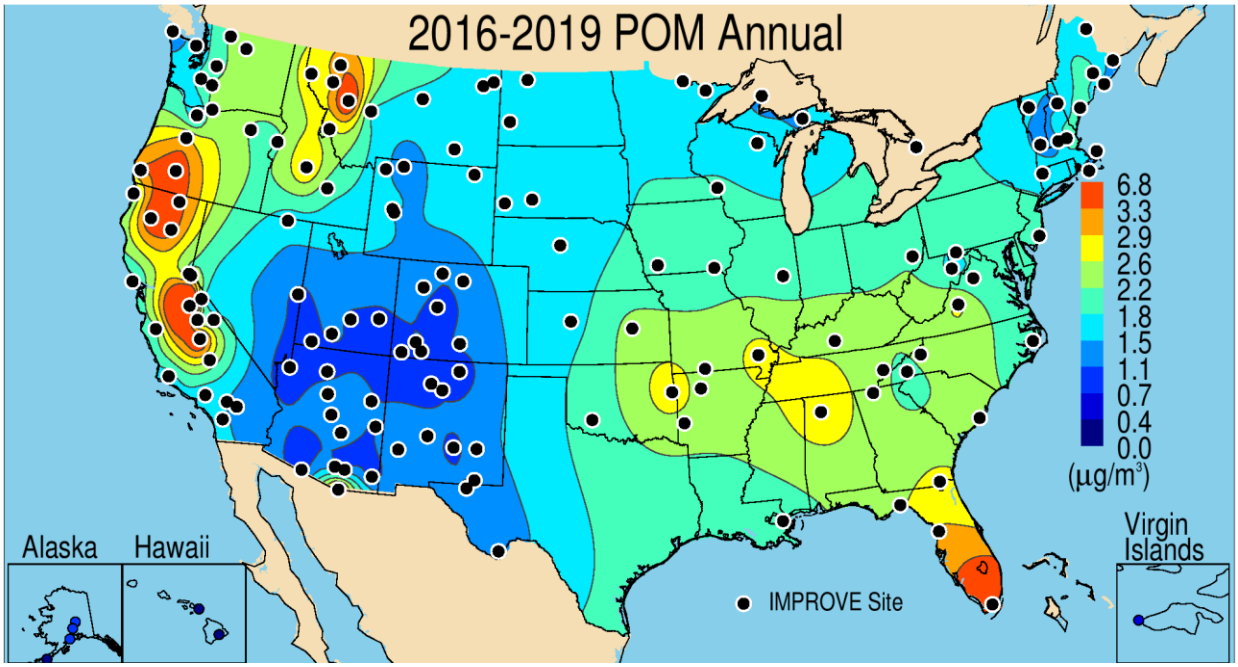

Figure 2.2.3a. IMPROVE 2016–2019 $PM_{2.5}$ particulate organic matter (POM) annual mean mass concentrations (µg m^{-3}).

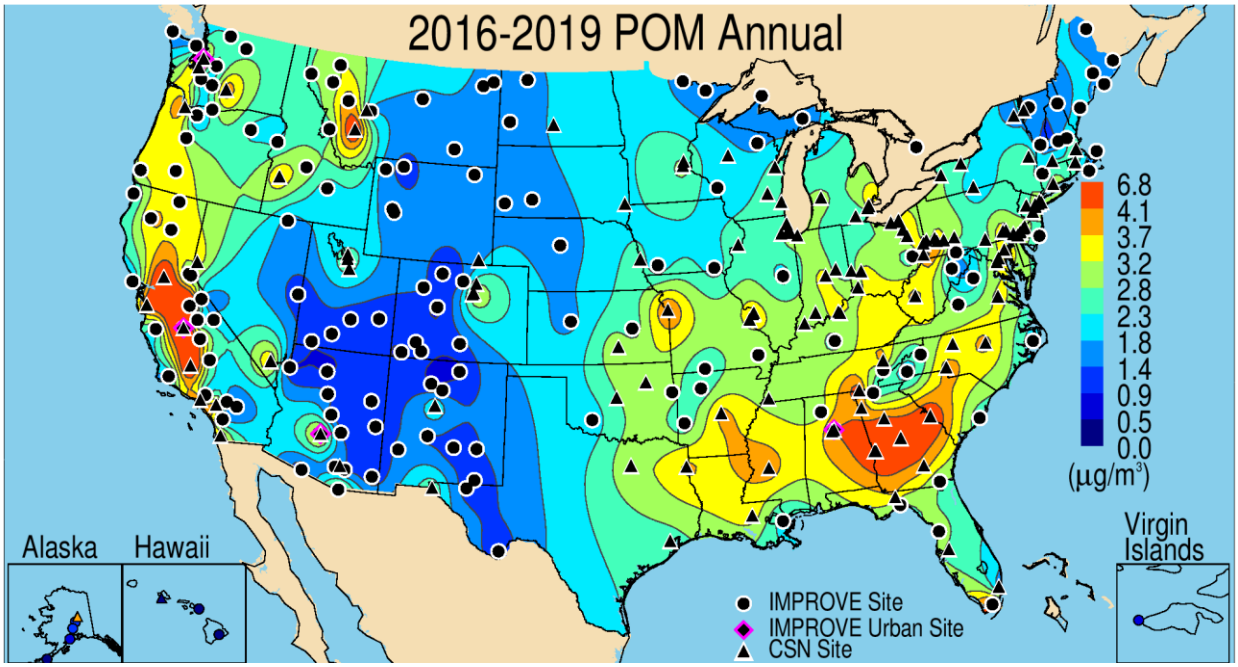

Figure 2.2.3b. IMPROVE and CSN 2016–2019 $PM_{2.5}$ particulate organic matter (POM) annual mean mass concentrations (µg m^{-3}).

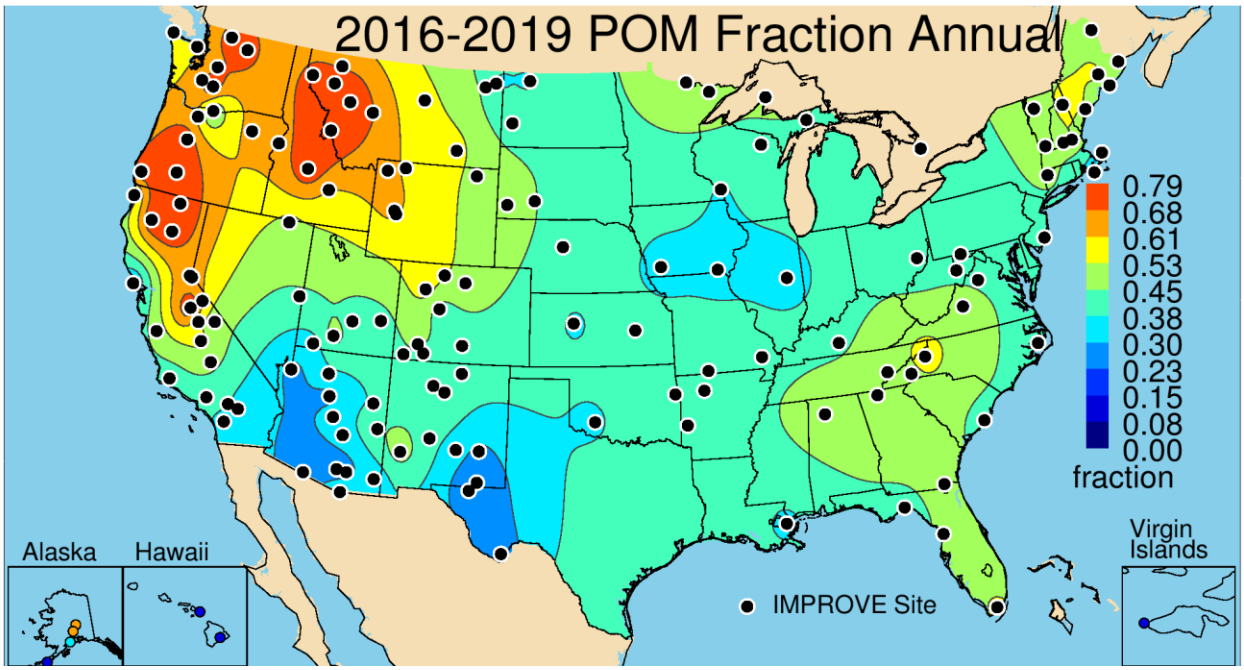

Figure 2.2.3c. IMPROVE 2016–2019 annual mean fraction contributions of particulate organic matter (POM) to $PM_{2.5}$ reconstructed fine mass (RCFM).

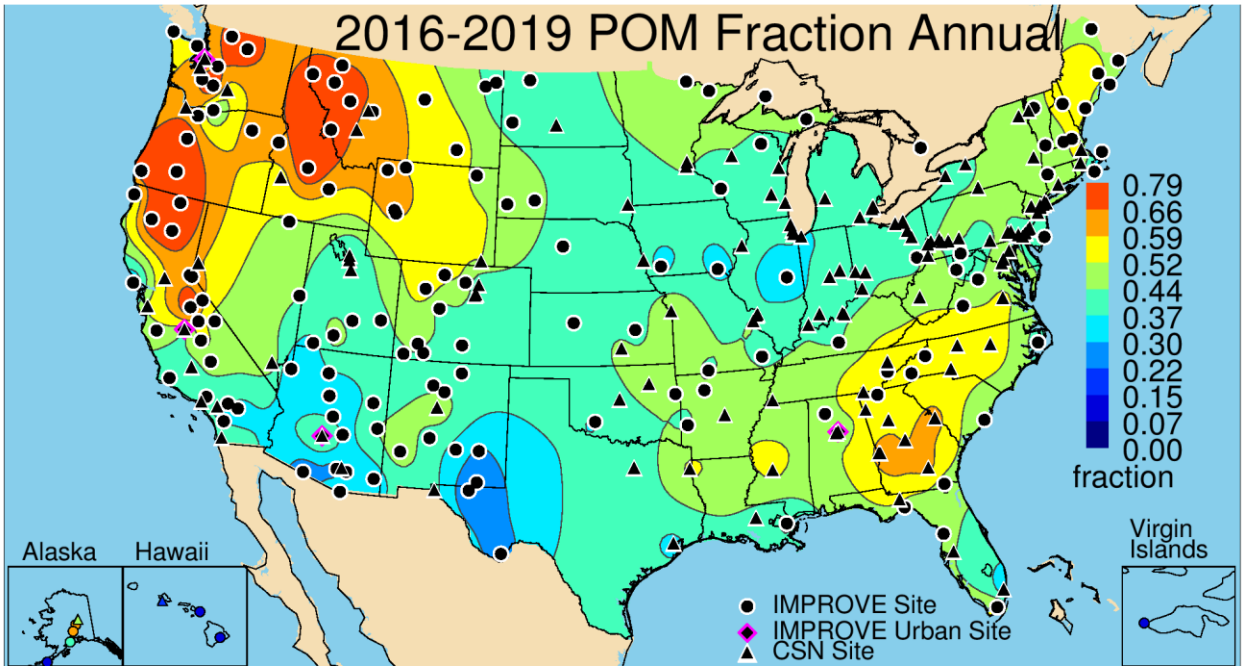

Figure 2.2.3d. IMPROVE and CSN 2016–2019 annual mean fraction contributions of particulate organic matter (POM) to $PM_{2.5}$ reconstructed fine mass (RCFM).

2.2.4 $PM_{2.5}$ Elemental Carbon Mass

EC, also referred to as light absorbing carbon or black carbon depending on the measurement method, is emitted directly from incomplete combustion of fossil fuels or biomass (e.g., Bond et al., 2013). EC as reported here is determined through thermal optical analysis (see Section 1.2.2), and Malm et al. (2020) (and references therein) indicated that the analysis can

inadvertently apportion some of the EC to OC, leading to underestimations of EC, depending on analysis conditions.

The IMPROVE rural 2016–2019 annual mean EC concentrations ranged from 0.02 μg m^{-3} in Haleakala Crater NP, Hawaii (HACR1), to 0.89 μg m^{-3} in Nogales, Arizona (NOGA1). The high annual mean concentration at Nogales was an outlier relative to sites in the rest of the Southwest and Intermountain West, where concentrations were typically around 0.1 μg m^{-3}. The IMPROVE site in Nogales is located on the edge of town near the border with Mexico and may experience impacts from Mexico. The EC seasonal pattern in Nogales reflects urban sources that typically peak in winter, and therefore the site may not represent typical rural EC seasonality and sources. The next-highest annual mean concentration occurred at Chassahowitzka National Wildlife Refuge (NWR) in Florida (0.34 μg m^{-3}, CHAS1), likely due to fire impacts. Farther west, EC concentrations were higher at sites in California and the Northwest (~0.25 μg m^{-3}). Most of the central and eastern United States also had higher annual mean concentrations (>0.25 μg m^{-3}; see Figure 2.2.4a).

Urban CSN EC concentrations were generally higher than at IMPROVE sites (maximum of 1.43 μg m^{-3} in Liberty, Pennsylvania, 420030064). Regionally, urban EC concentrations were highest at sites in the East; however, most impacts of EC were local in extent. Several hot spots occurred in major urban areas, for example, near Denver, Colorado; Butte, Montana; Las Vegas, Nevada, and several sites in the Central Valley of California (Figure 2.2.4b). The urban hotspots were indicative of local urban EC emissions (e.g., mobile sources or local residential wood burning) rather than regional sources like biomass combustion from controlled or wild fires. The steep spatial gradient surrounding the hotspots of EC in Figure 2.2.4b indicated that the spatial extent of the impact was small with low regional impacts.

EC was a minor contributor to RCFM at most IMPROVE sites around the United States (Figure 2.2.4c). The highest EC fractions occurred at sites in the Northwest and Northeast (0.05–0.09), with the maximum of 0.09 at Nogales, Arizona (NOGA1), where the highest annual mean concentrations also occurred in the IMPROVE network. The Nogales site was an outlier in the region where most sites had EC fractions of 0.03–0.04. The second-highest EC mass fraction occurred at Londonderry, New Hampshire (LOND1, 0.07).The lowest contributions occurred at Virgin Islands NP (0.01, VIIS1).

Many of the urban CSN sites that had elevated annual mean EC concentrations also had higher EC fractions (>0.10; see Figure 2.2.4.d). The highest urban EC fraction (0.16) occurred at Charleston, West Virginia (540390020) and the lowest (0.04) occurred at Kapolei, Hawaii (150030010). In general, urban sites had higher EC fractions, and this influence appeared to be fairly localized.

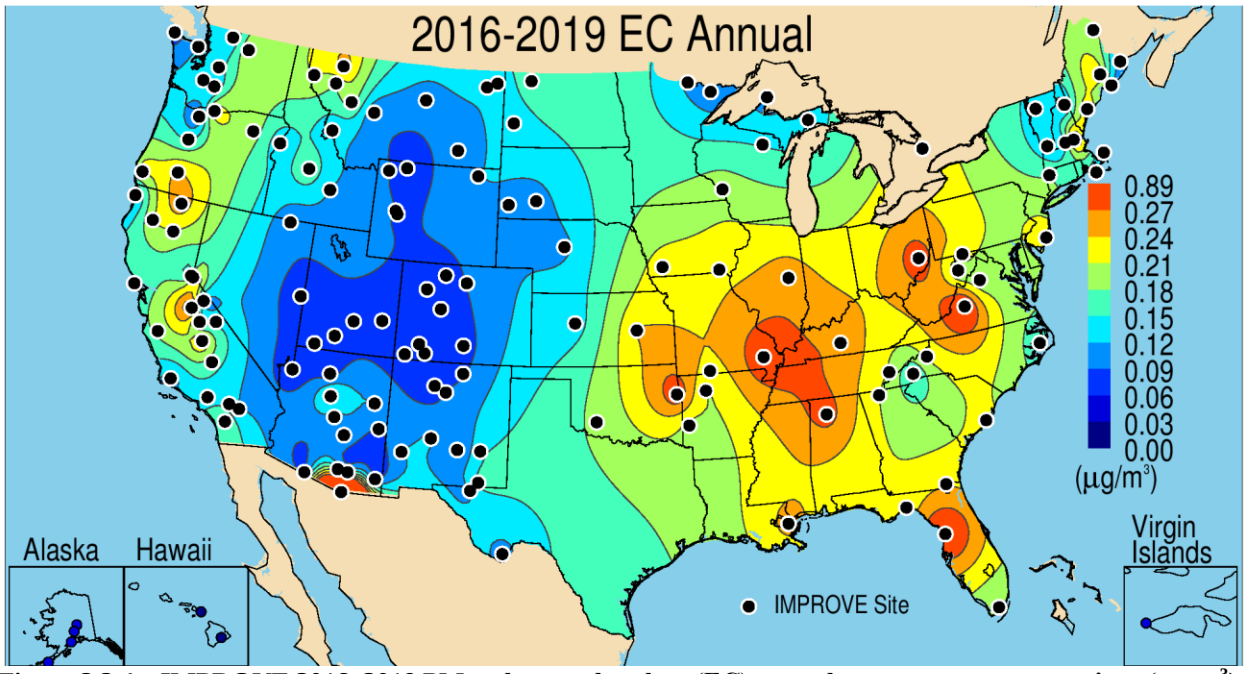

Figure 2.2.4a. IMPROVE 2016–2019 $PM_{2.5}$ elemental carbon (EC) annual mean mass concentrations (µg m^{-3}).

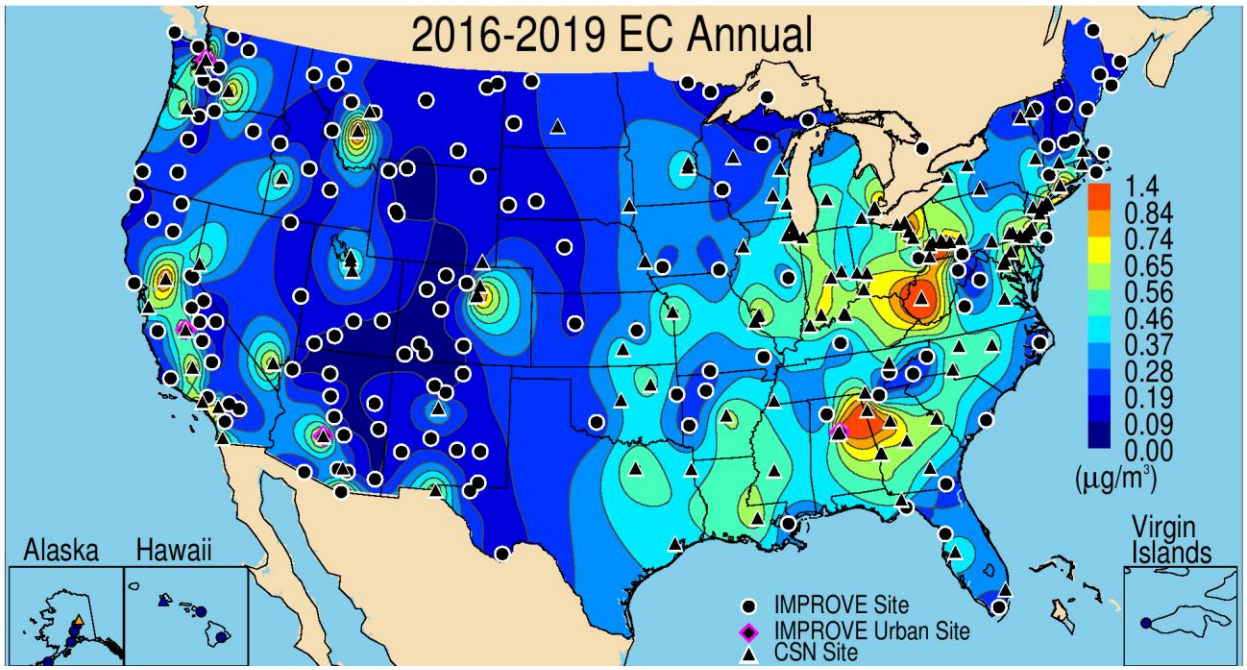

Figure 2.2.4b. IMPROVE and CSN 2016–2019 $PM_{2.5}$ elemental carbon (EC) annual mean mass concentrations (µg m^{-3}).

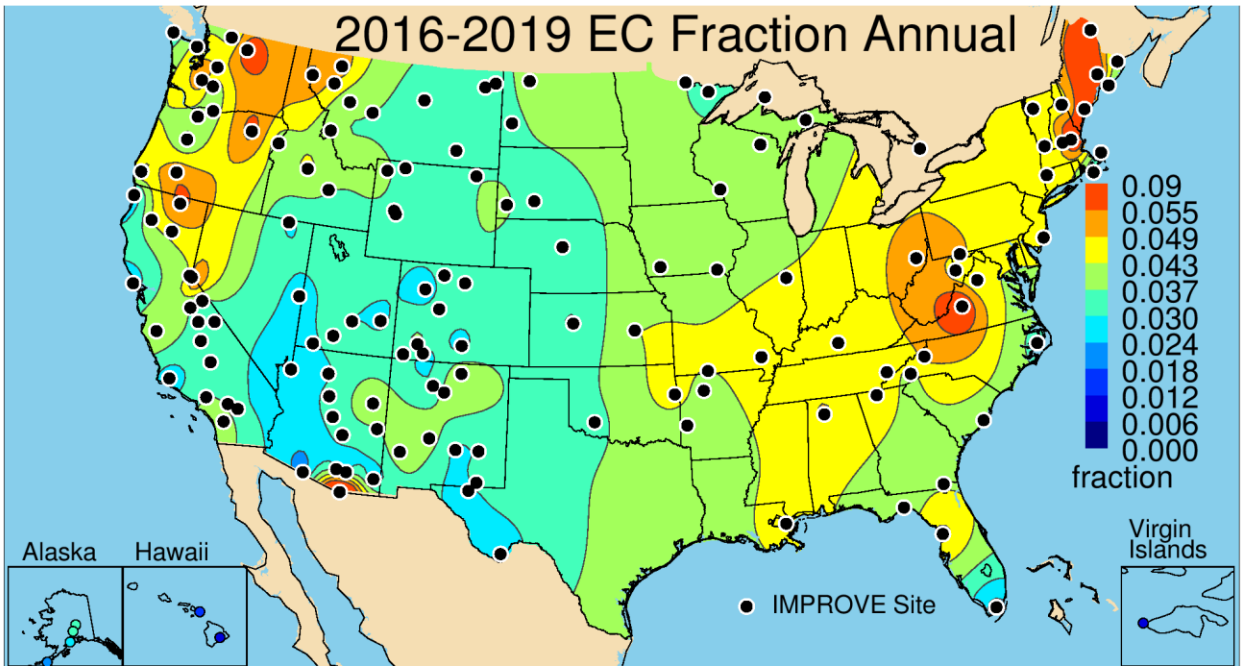

Figure 2.2.4c. IMPROVE 2016–2019 annual mean fraction contributions of elemental carbon (EC) to $PM_{2.5}$ reconstructed fine mass (RCFM).

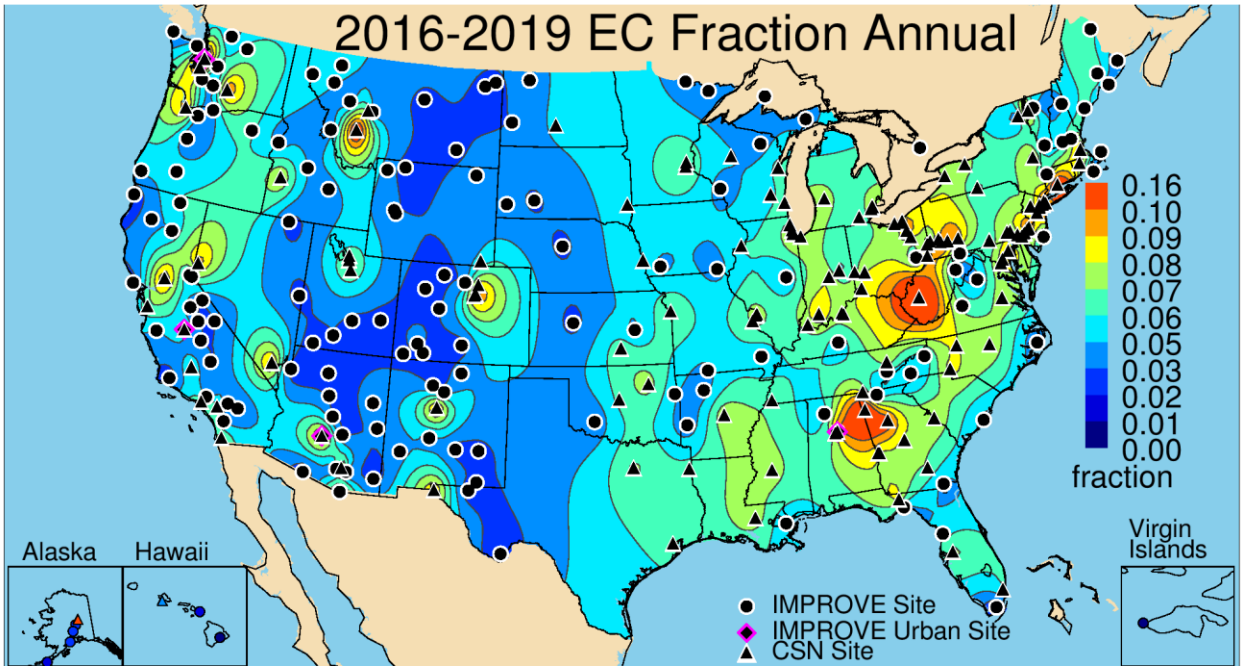

Figure 2.2.4d. IMPROVE and CSN 2016–2019 annual mean fraction contributions of elemental carbon (EC) to $PM_{2.5}$ reconstructed fine mass (RCFM).

2.2.5 Filter Light Absorption (f_{abs})

Black carbon strongly absorbs visible light (Moosmüller et al., 2009; Bond et al., 2013) and although f_{abs} is a measure of all light absorbing particles on the $PM_{2.5}$ Teflon filter, black carbon is likely the main contributor given its strong absorbing properties. However, fine mineral dust containing iron oxides is known to absorb in the visible spectrum, (Moosmüller et al., 2012;

White et al., 2016); therefore it is expected that absorption from iron oxides will also contribute to f_{abs}. Measurements of f_{abs} are currently available only for the IMPROVE network and only on $PM_{2.5}$ filters.

The 2016–2019 annual mean f_{abs} tends to follow EC spatial patterns since most of the filter absorption is likely due to EC (Figure 2.2.5). The highest annual mean f_{abs} occurred in Nogales, Arizona (10.5 Mm^{-1}, NOGA1) and the lowest occurred in Hawaii Volcanoes NP, Hawaii (0.21 Mm^{-1}, HAVO1). The highest EC concentration also occurred at Nogales and the lowest EC concentration occurred in Hawaii (Haleakala NP). The second-highest annual mean f_{abs} occurred at Chassahowitzka NWR in Florida (CHAS1, 4.1 Mm^{-1}), likely due to impacts from biomass smoke. Biomass smoke also likely influenced higher f_{abs} at sites along the West Coast. Somewhat elevated f_{abs} occurred in the Southwest, perhaps due to the role of iron absorption in dust. The eastern United States was associated with elevated f_{abs} across large regions, very similar to the observed EC pattern.

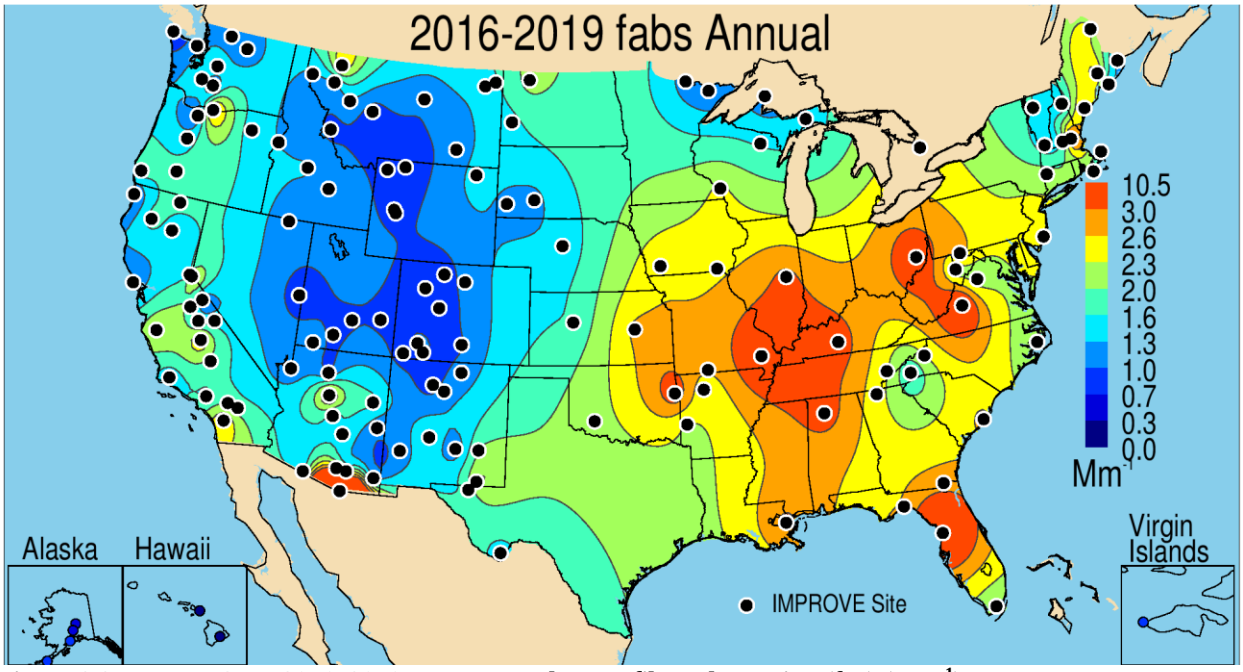

Figure 2.2.5. IMPROVE 2016–2019 $PM_{2.5}$ annual mean filter absorption (f_{abs}) (Mm^{-1}).

2.2.6 $PM_{2.5}$ Fine Dust Mass

Sources of mineral dust in the atmosphere include entrainment from deserts, paved and unpaved roads, agricultural activity, construction, and fire. Deposition of dust usually corresponds to large particles that settle near their source regions, although there are many exceptions. The seasonal and spatial variability of dust in the United States is influenced by both local, regional, and long-range transport. Several studies have shown that contributions of Asian dust to U.S. fine dust concentrations can be significant episodically, affecting aerosol concentrations and mineralogy across the United States, typically in the spring (e.g., Husar et al., 2001; Prospero et al., 2002; Creamean et al., 2014; Hand et al., 2017; Kim et al., 2021). Transport of North African dust to the United States occurs regularly in summer, affecting aerosol concentrations in the Virgin Islands, the eastern and southeastern United States (Perry et

al., 1997; Hand et al., 2017; Bozlaker et al., 2019; Prospero et al., 2021), and even as far west as Big Bend NP, Texas (Hand et al., 2002). Dust concentrations in desert regions of the Southwest are expected to be higher due to the impacts of local sources as well as transboundary transport from the Chihuahuan desert in Mexico, especially in winter and spring (Rivera et al., 2009; Tong et al., 2012; Hand et al., 2016; 2017). Dust in the central United States is influenced by agricultural activity (Hand et al., 2017; Pu and Ginoux, 2018; Lambert et al., 2020).

FD as characterized by $PM_{2.5}$ samplers most likely corresponds to the fine tail of the coarse mode. Variability in dust concentrations could be due to changes in the magnitudes of mass concentrations for a given size mode or to a shifting size distribution that results in more or less mass available in the fine-mode size range. Due to the spatial and temporal variability in dust sources, it is very difficult to characterize an appropriate aerosol dust composition for each measurement site. FD mass concentrations are therefore estimated by a general method that sums the oxides of elements that are typically associated with soil (Al_2O_3, SiO_2, CaO, K_2O, FeO, Fe_2O_3, TiO_2), with a correction for other compounds such as MgO, Na_2O, H_2O, and carbonates (Malm et al., 1994). Elemental concentrations are multiplied by factors that represent the mass concentrations of the oxide forms. Several corrections are also made. Molar concentrations of iron are assumed to be equally abundant in the forms of FeO and Fe_2O_3. Potassium has a nonsoil contribution from biomass smoke, so the soil potassium is estimated by using Fe as a surrogate, or [K] = 0.6×[Fe]. The original formula for computing FD concentrations included a multiplier of 1.16 to account for missing compounds (Table 2.1). As discussed in Section 2.1, IMPROVE FD concentrations in this report are derived from the original formula and multiplied by 1.15 to reflect an underestimation of FD identified by multiple linear regression analyses (see Appendix 2.1). CSN FD concentrations are not multiplied by this factor; however, recall that comparisons of IMPROVE and CSN data at collocated sites suggested that relative biases of 20% in FD concentrations existed, with higher IMPROVE concentrations. This bias is likely due to the differences in the sharpness of size cut points of the samplers. Given these uncertainties, the aggregation of IMPROVE and CSN FD concentrations should be interpreted as semiquantitative.

The patterns observed in the 2016–2019 annual mean rural IMPROVE FD concentrations were reflective of dominant seasons of elevated dust concentrations, namely the Southwest during spring and the Southeast during summer (Hand et al., 2017). The highest annual mean concentrations occurred at sites in the Southwest, with the highest at Nogales, Arizona (3.11 μg m^{-3}, NOGA1), and followed a lobed spatial pattern determined by the terrain of the Mogollon Plateau. Concentrations at other sites in Arizona ranged from 1.3 to 3.1 μg m^{-3}. The second-highest annual mean FD concentration occurred at Sycamore Canyon, Arizona (3.10 μg m^{-3}, SYCA2). Sites around the Colorado Plateau as well as sites in southern New Mexico and western Texas had concentrations near 1 μg m^{-3} (see Figure 2.2.6a). Unlike other species with spatial gradients along the east/west orientation, FD gradients extended north/south. The concentrations at northern sites tended to be lower (~0.5 μg m^{-3}), and the lowest rural annual mean FD concentration occurred at the Makah Tribe site in Washington (0.07 μg m^{-3}, MAKA1).

Although the CSN FD concentrations were biased low relative to IMPROVE concentrations, the spatial patterns in combined urban and rural FD generally agreed, with higher concentrations at sites in the Southwest (Figure 2.2.6b). There were several urban hot spots with elevated FD concentrations. For example, the CSN sites at Denver, Colorado; Las Vegas, Nevada; St. Louis, Missouri; Dallas, Texas; and sites in the Central Valley of California had

higher FD concentrations relative to surrounding areas. The highest annual mean FD concentration (2.07 μg m^{-3}) occurred at El Paso, Texas (481410044), and the lowest concentration in the CSN network was measured in northeastern New York (0.17 μg m^{-3}, Wilmington, 360310003).

FD contributed a substantial fraction of RCFM at rural sites in the western United States (Figure 2.2.6c), where annual mean fractions ranged from 0.25 to 0.55. The highest fraction (0.55) occurred at Sycamore Canyon, Arizona (0.55, SYCA2). At sites across the Northwest and the eastern United States, annual mean FD contributions were typically <0.15. The lowest annual mean FD fractional contribution occurred at Redwood NP, California (0.03, REDW1). The combined IMPROVE and CSN annual mean FD fraction spatial pattern was very similar to that of IMPROVE alone, with higher contributions in the Southwest (Figure 2.2.6d). At sites across the Northwest and eastern United States, the urban FD fraction was typically <0.1. The highest CSN annual mean FD fraction occurred in El Paso, Texas (0.29, 481410044), similar to the highest CSN FD concentration. The lowest fraction occurred at Tacoma, Washington (0.04, 530530029).

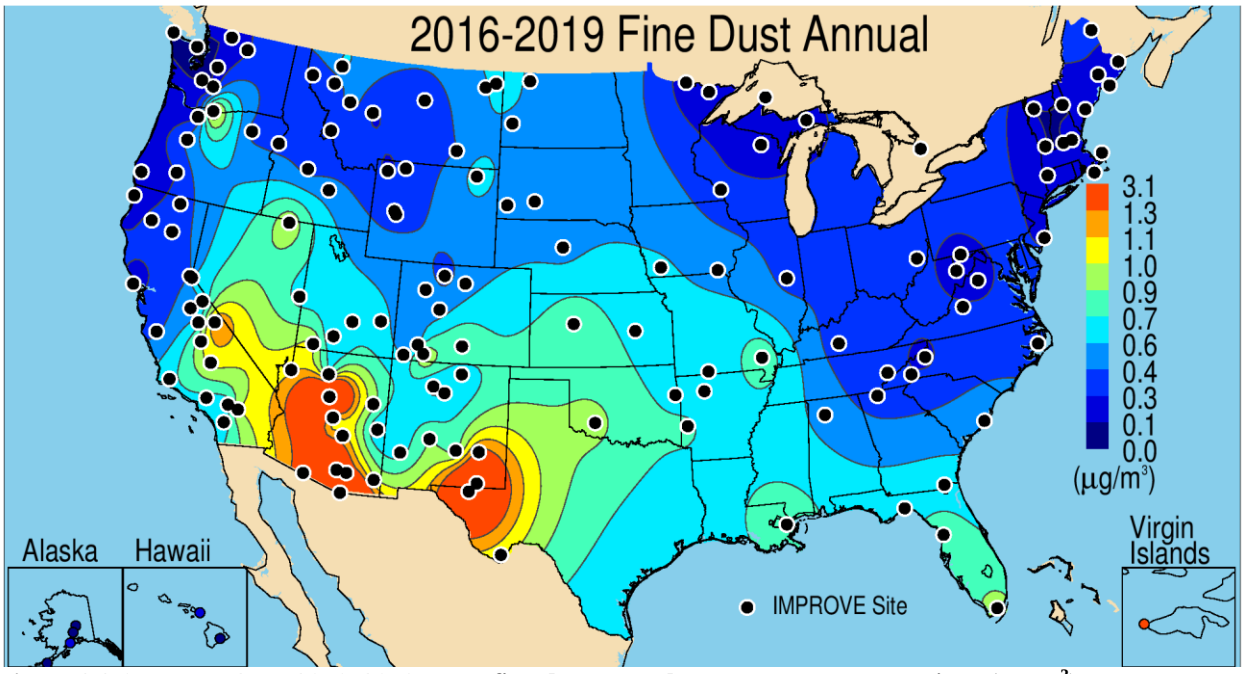

Figure 2.2.6a. IMPROVE 2016–2019 $PM_{2.5}$ fine dust annual mean mass concentrations (μg m^{-3}).

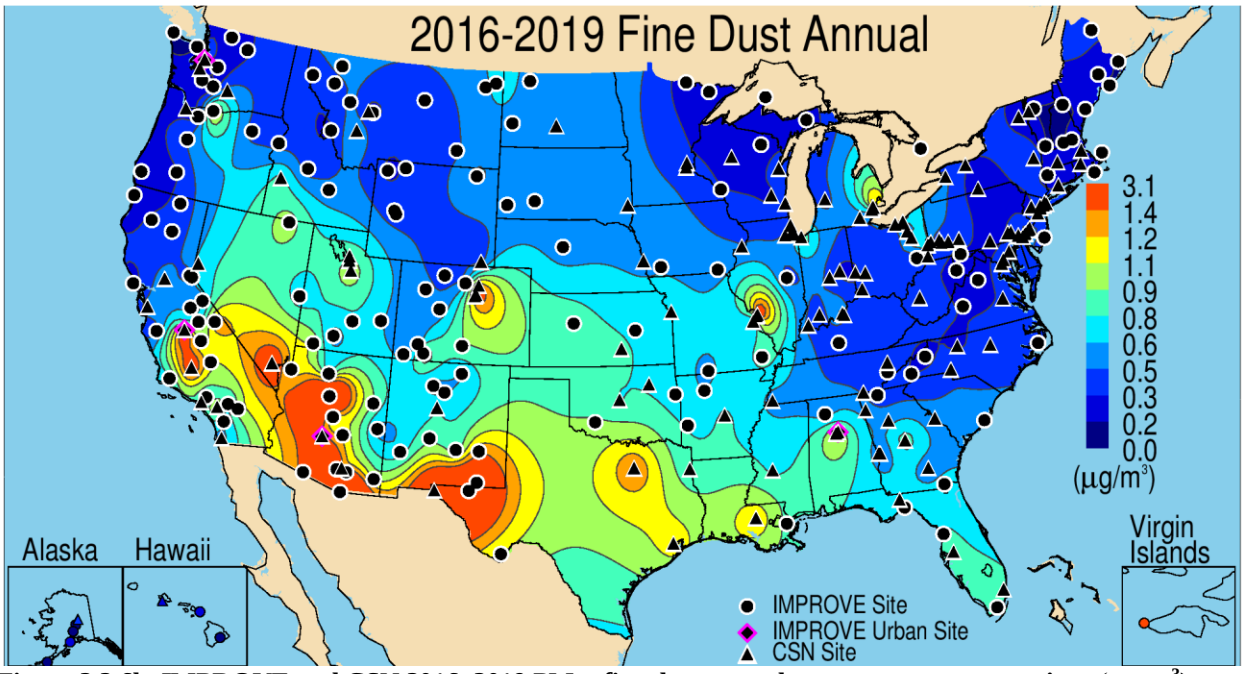

Figure 2.2.6b. IMPROVE and CSN 2016–2019 $PM_{2.5}$ fine dust annual mean mass concentrations (µg m^{-3}).

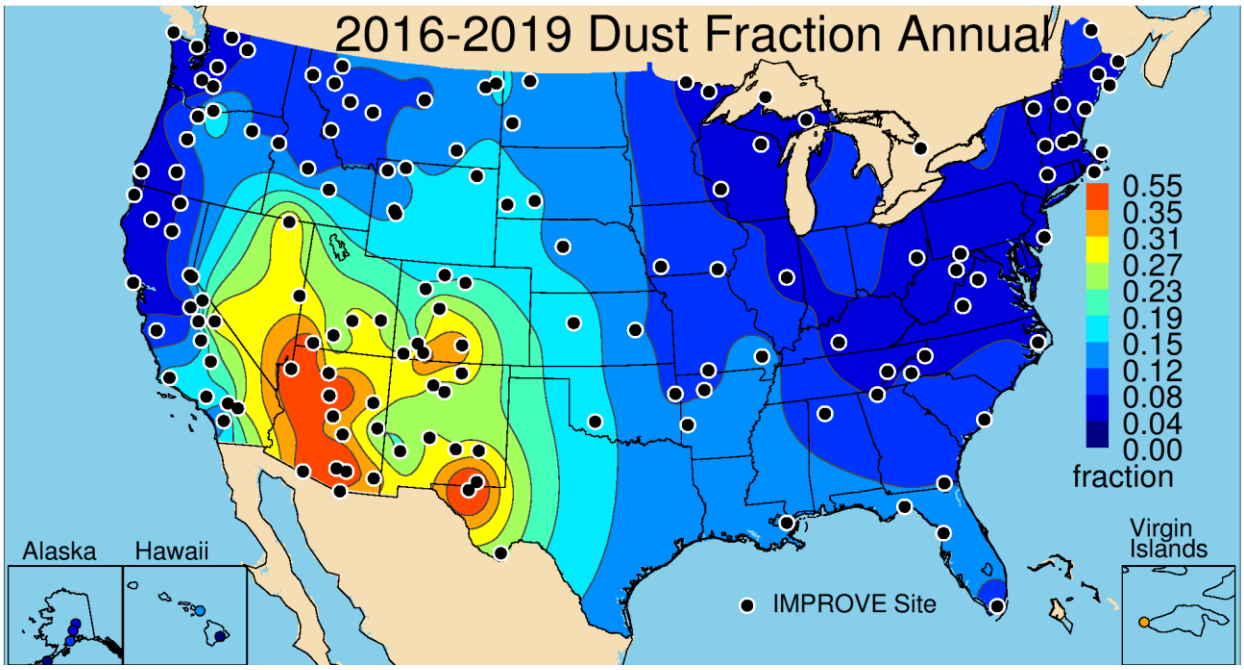

Figure 2.2.6c. IMPROVE 2016–2019 annual mean fraction contributions of fine dust to $PM_{2.5}$ reconstructed fine mass (RCFM).

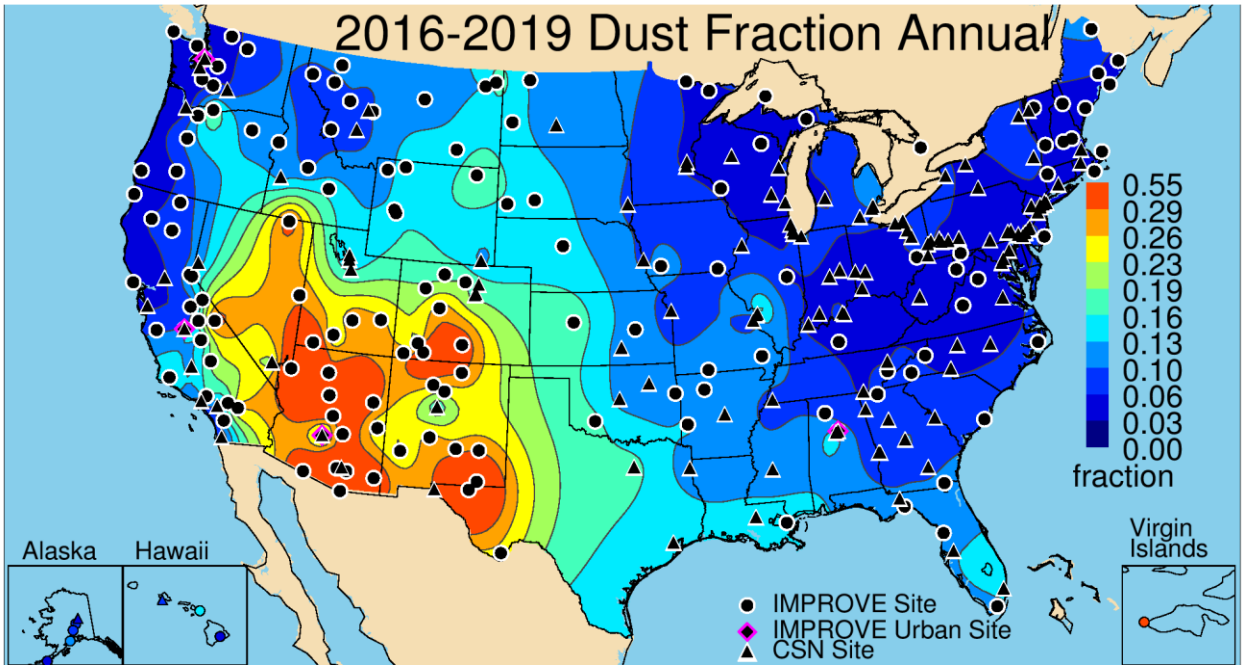

Figure 2.2.6d. IMPROVE and CSN 2016–2019 annual mean fraction contributions of fine dust to $PM_{2.5}$ reconstructed fine mass (RCFM).

2.2.7 $PM_{2.5}$ Sea Salt Mass

SS can be a significant fraction of the RCFM at many coastal locations, as well as contribute significantly to light scattering (e.g., Lowenthal and Kumar, 2006; Murphy et al., 2019). SS concentrations are typically computed from SS markers like sodium ion, chloride ion, or combination of ions (White, 2008). Difficulties in computing SS from data from the IMPROVE network arise because positive ions are not analyzed; therefore sodium ion data (the strongest indicator of SS) are not available. Elemental sodium data are available from X-ray fluorescence (XRF) analyses; however, sensitivity issues regarding poor detection of Na result in large uncertainties (White, 2008). Issues also arise when using the chloride ion or chlorine to estimate SS, because the reaction of gaseous nitric acid with SS produces sodium nitrate particles and the release of gaseous hydrochloric acid. The depletion of chloride during this reaction results in an underestimation of SS when using chloride to compute it. However, given these limitations, it was proposed by Pitchford et al. (2007) that calculations for reconstructing mass in the IMPROVE algorithm include SS by multiplying the chloride ion (Cl^-) by 1.8 (SS is 55% Cl by weight as defined by the composition of seawater). Because the chloride ion only began being reported for the CSN in February 2017, SS is computed using a 1.8 factor multiplied by chlorine as measured by XRF. Comparisons of SS concentrations between collocated CSN and IMPROVE sites (see Section 1.4) suggested that IMPROVE concentrations were up to three times higher on average compared to CSN, with a relative bias of 63%. Given these disparities in concentrations, the integration of CSN and IMPROVE SS data should be interpreted with caution.

The IMPROVE sites with the highest 2016–2019 annual mean SS concentrations were along coastal regions (Figure 2.2.7a). Concentrations at rural IMPROVE sites ranged from 0.01 μg m^{-3} at North Absaroka, Wyoming (NOAB1), to 2.29 μg m^{-3} at Point Reyes National Seashore

(NS), California (PORE1). Outside of coastal regions, SS concentrations were low (<0.10 µg m^{-3}). The spatial patterns were generally similar when aggregating IMPROVE and CSN data (Figure 2.2.7b). The minimum annual mean concentration was essentially zero (-0.0004 µg m^{-3}) at Cheyenne, Wyoming (560210100), and the maximum SS concentration of 0.83 µg m^{-3} occurred in Kapolei, Hawaii (150030010).

At the IMPROVE site at Simeonof, Alaska (SIME1), SS fractional contributions to RCFM was 0.49, compared to the minimum contribution at Monture, Montana (0.02, MONT1) (Figure 2.2.7c). Similar to the spatial distribution of SS concentrations, fractional contributions were highest at coastal sites and at sites in Hawaii, Alaska, and the Virgin Islands. These spatial patterns also held for combined IMPROVE and CSN fraction contributions (Figure 2.2.7d). The highest annual mean SS contribution (0.30) at CSN sites occurred at Kapolei, Hawaii (150032010), where the highest concentration was observed. The lowest contribution (zero) also occurred at Cheyenne, Wyoming (560210100).

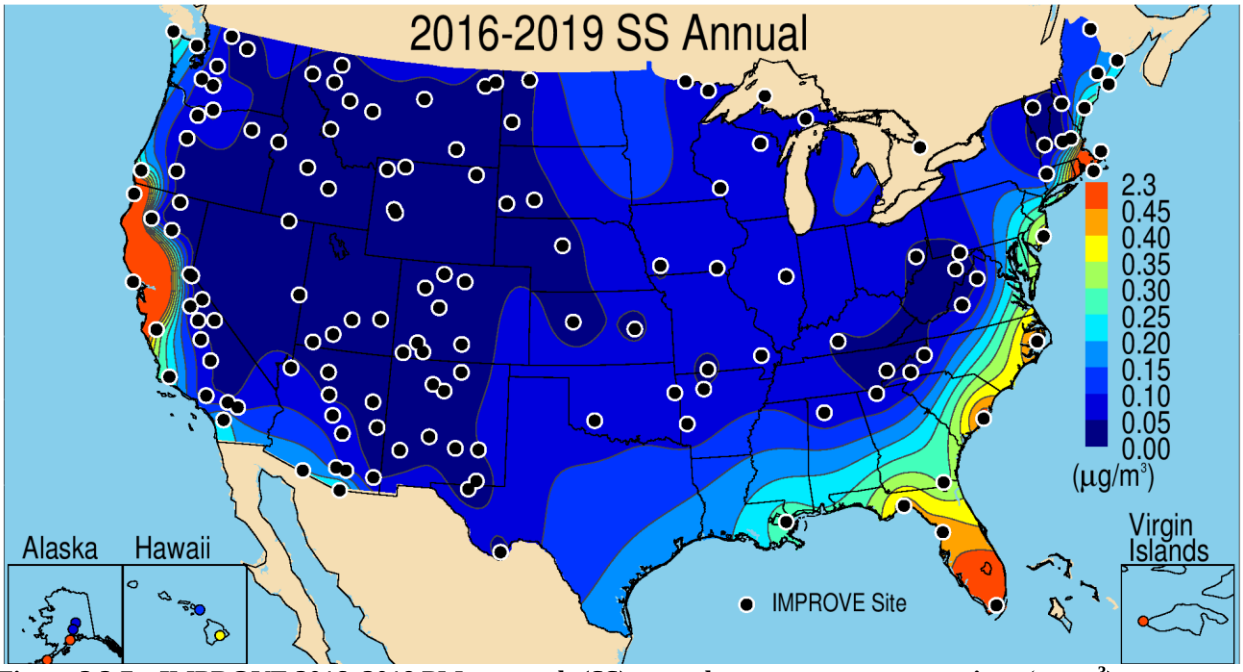

Figure 2.2.7a. IMPROVE 2016–2019 $PM_{2.5}$ sea salt (SS) annual mean mass concentrations (µg m^{-3}).

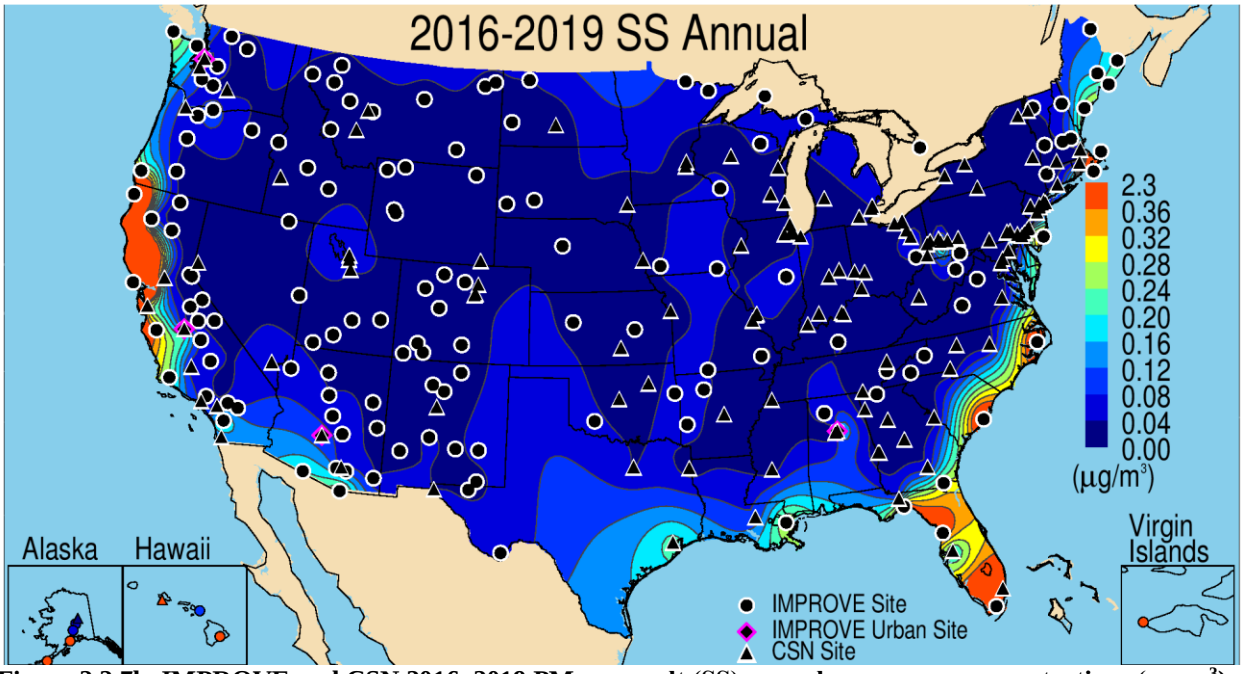

Figure 2.2.7b. IMPROVE and CSN 2016–2019 $PM_{2.5}$ sea salt (SS) annual mean mass concentrations (µg m^{-3}).

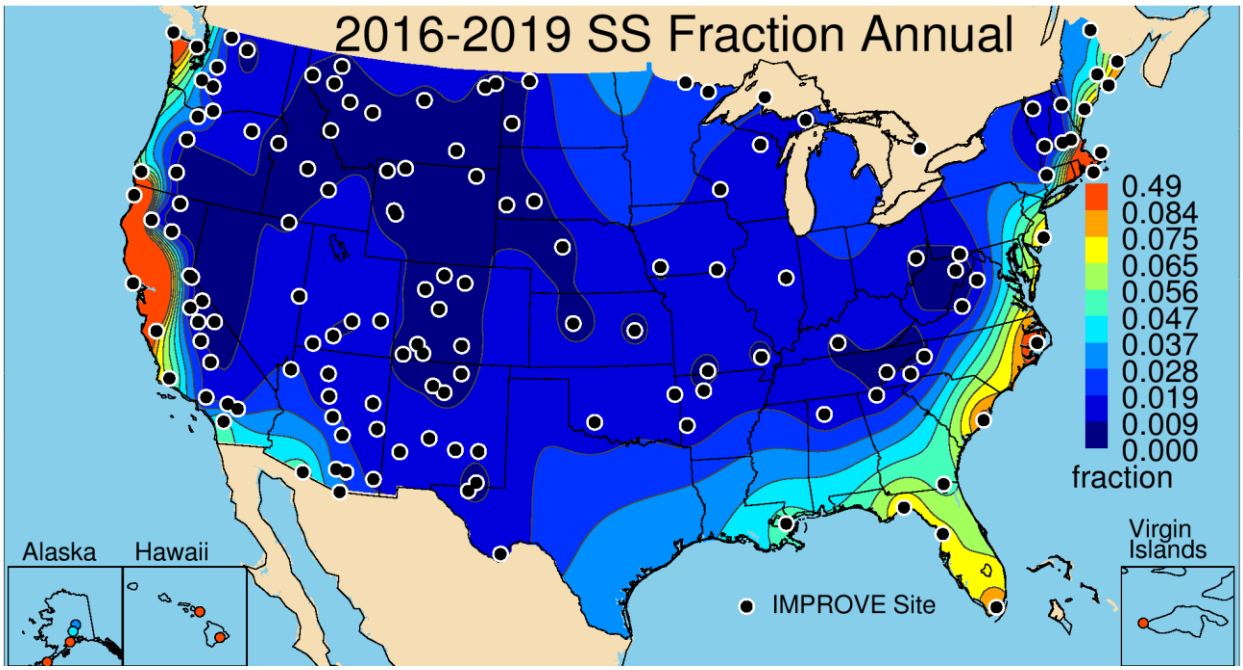

Figure 2.2.7c. IMPROVE 2016–2019 annual mean fraction contributions of sea salt to $PM_{2.5}$ reconstructed fine mass (RCFM).

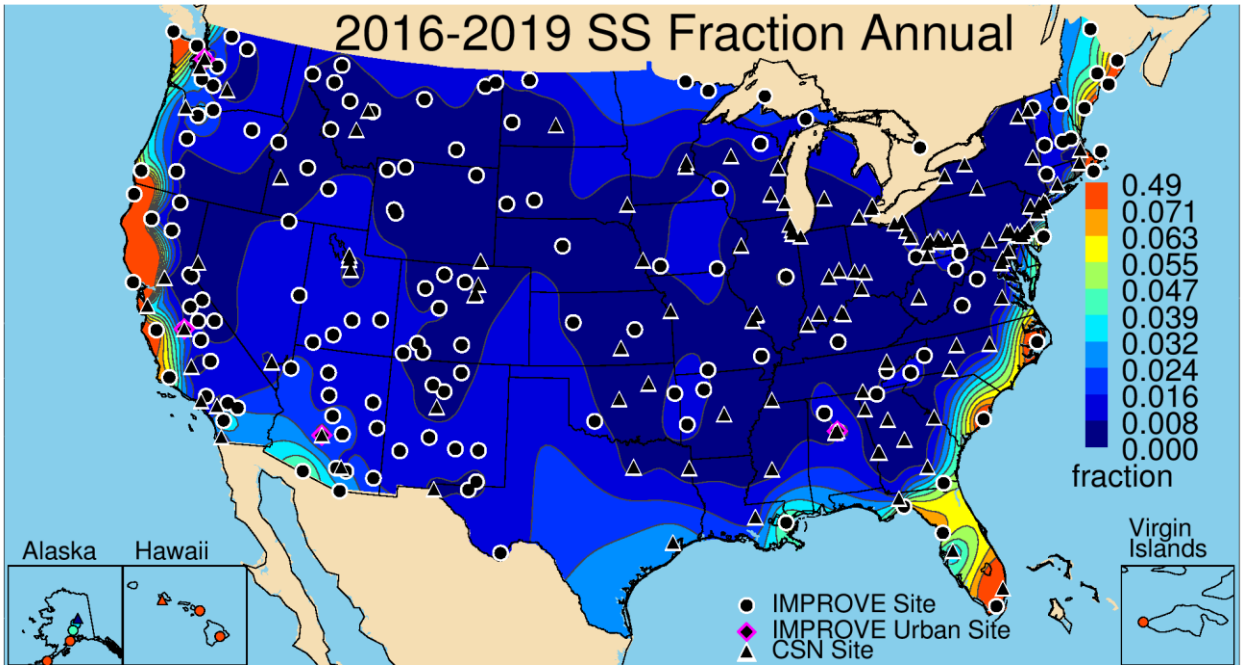

Figure 2.2.7d. IMPROVE and CSN 2016–2019 annual mean fraction contributions of sea salt (SS) to $PM_{2.5}$ reconstructed fine mass (RCFM).

2.2.8 $PM_{2.5}$ Gravimetric Fine Mass

Gravimetric $PM_{2.5}$ mass concentrations (FM) are determined by pre- and post-weighing of Teflon filters. Teflon filters have known sampling artifacts. For example, nitrate loss and volatilization of some organic species contribute to negative artifacts (e.g., Hering and Cass, 1999; Chow et al., 2005; Watson et al., 2009; Chow et al., 2010), while positive artifacts correspond to retention of water associated with hygroscopic species (Frank, 2006; Hand et al., 2019b). Due to budget considerations, at the end of 2014, gravimetric analysis was no longer performed on CSN filters. Instead, gravimetric $PM_{2.5}$ data from the EPA's FRM samplers at collocated CSN sites were used.

The spatial pattern of 2016–2019 annual mean IMPROVE FM concentrations reflected the combined patterns of annual mean concentrations of AS, AN, and POM (see Figure 2.2.8a). The highest IMPROVE annual mean FM concentrations occurred in Nogales, Arizona (8.55 μg m^{-3}, NOGA1), where the maximum f_{abs}, EC, and FD concentrations occurred. The second-highest annual mean FM occurred at Sequoia NP, California (7.52 μg m^{-3}, SEQU1). Sites in the central and eastern United States also had relatively high annual mean FM concentrations (>5.6 μg m^{-3}). In addition, sites in California's Central Valley had higher concentrations. The lowest FM concentrations occurred in the Intermountain West, and the lowest annual mean concentration occurred in Denali NP, Alaska (1.24 μg m^{-3}, DENA1).

The urban FM concentrations measured by the CSN network were somewhat higher than the IMPROVE concentrations, especially at sites in the central and eastern United States (Figure 2.2.8b). High annual mean urban FM was also observed at sites in the Central Valley of California, where the highest urban annual mean FM (13.57 μg m^{-3}) occurred at Fresno (060190011). Several hot spots of annual mean FM occurred at urban sites across the West, such

as Denver, Colorado; El Paso, Texas; Salt Lake City, Utah; Butte, Montana; and Yakima, Washington. The lowest CSN annual mean FM concentration (3.43 μg m^{-3}) occurred at White Face, New York (360310003).

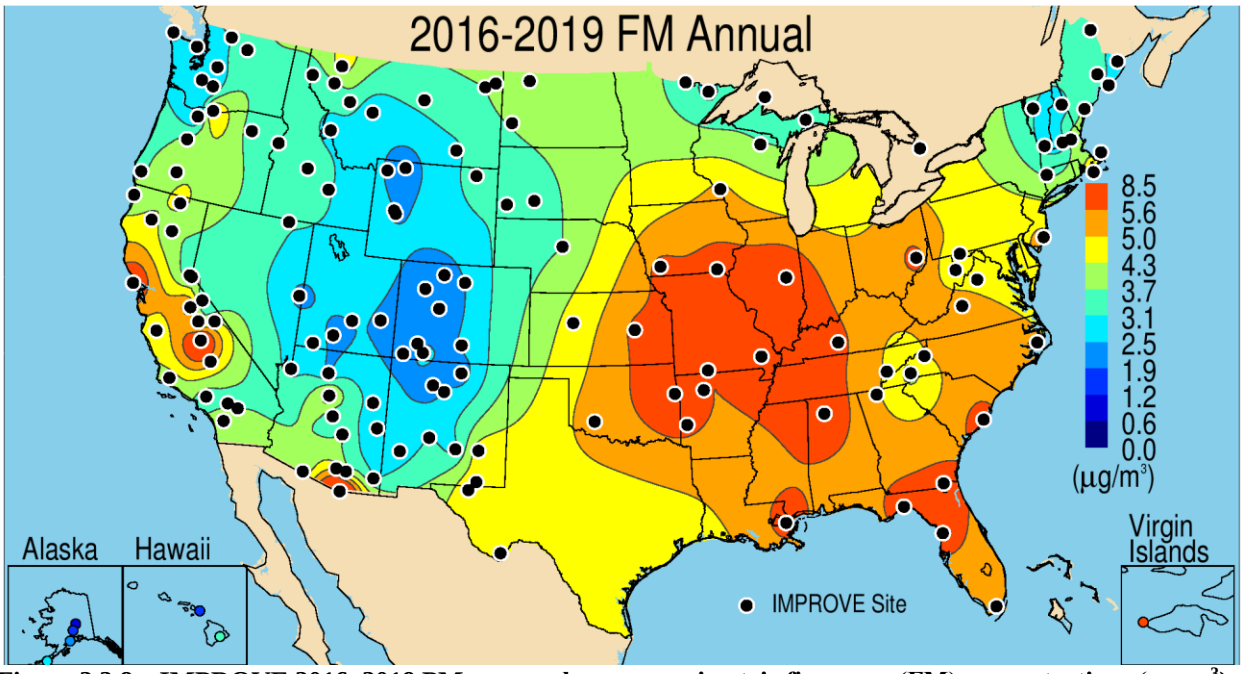

Figure 2.2.8a. IMPROVE 2016–2019 $PM_{2.5}$ annual mean gravimetric fine mass (FM) concentrations (μg m^{-3}).

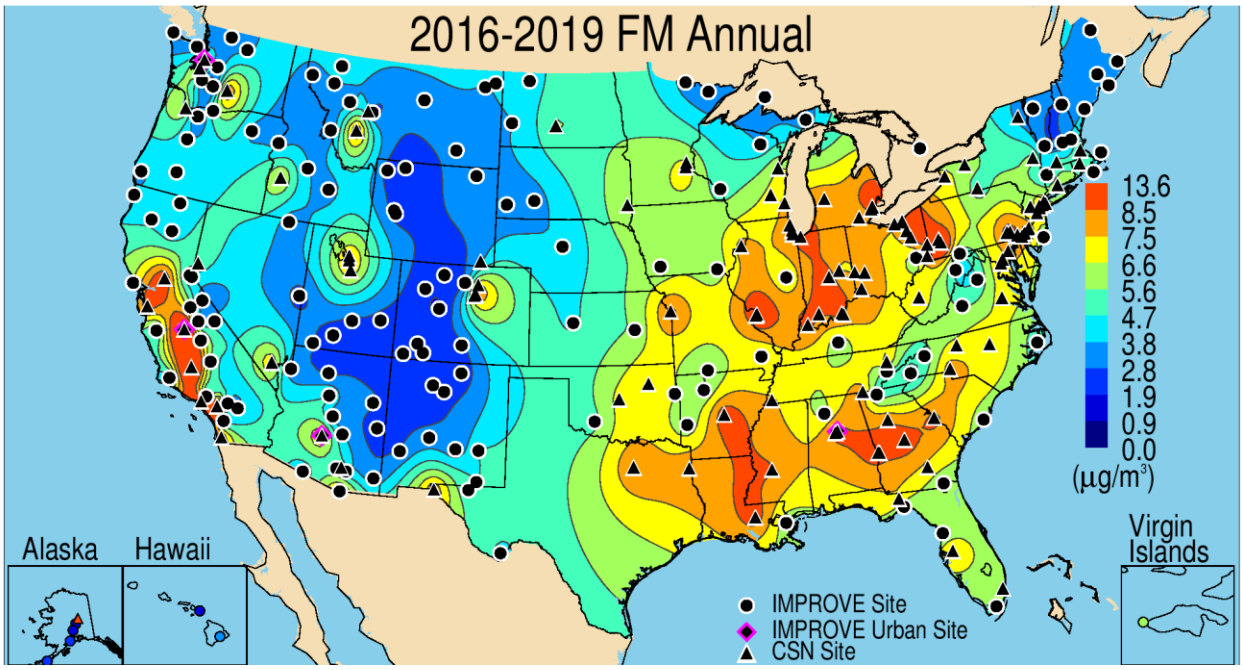

Figure 2.2.8b. IMPROVE and CSN 2016–2019 $PM_{2.5}$ annual mean gravimetric fine mass (FM) concentrations (μg m^{-3}).

2.2.9 $PM_{2.5}$ Reconstructed Fine Mass

RCFM is the sum of AS, AN, POM, EC, FD, and SS. RCFM should equal FM if the assumptions regarding molecular forms of species are appropriate and if there are minimal biases associated with the measurements.

The spatial patterns of annual mean RCFM generally followed those of FM patterns, although different scales may affect the appearance (Figure 2.2.9a). For example, sites with highest annual mean RCFM were in the central United States and along the Central Valley of California. The maximum annual mean RCFM also occurred in Nogales, Arizona (9.34 μg m^{-3}), as did the maximum for FM. The second-highest RCFM occurred at Everglades NP, Florida (8.7 μg m^{-3}, EVER1). In the continental United States, sites in the Intermountain West had the lowest annual mean RCFM. The minimum annual mean RCFM occurred in Haleakala Crater NP, Hawaii (1.15 μg m^{-3}, HACR1). The urban CSN annual mean RCFM ranged from 2.75 μg m^{-3} at Kapolei, Hawaii (150030010), to 14.21 μg m^{-3} at Bakersfield in California's Central Valley (060290014) (Figure 2.2.9b).

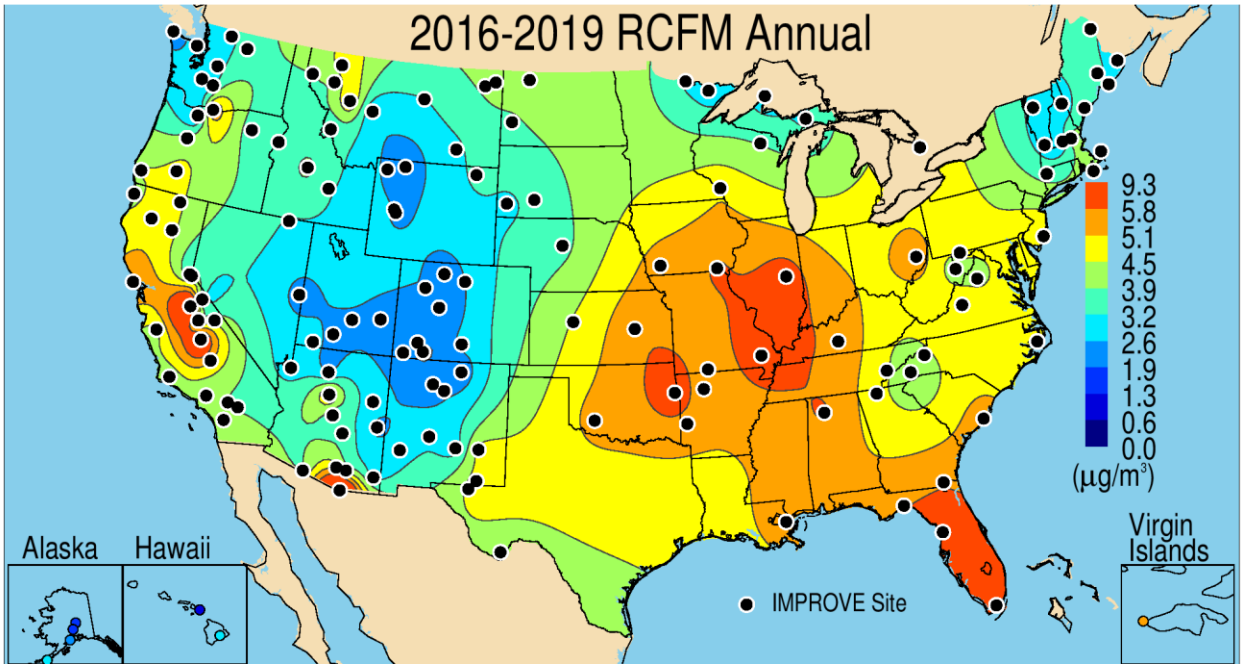

Figure 2.2.9a. IMPROVE 2016–2019 $PM_{2.5}$ annual mean reconstructed fine mass (RCFM) concentrations (μg m^{-3}).

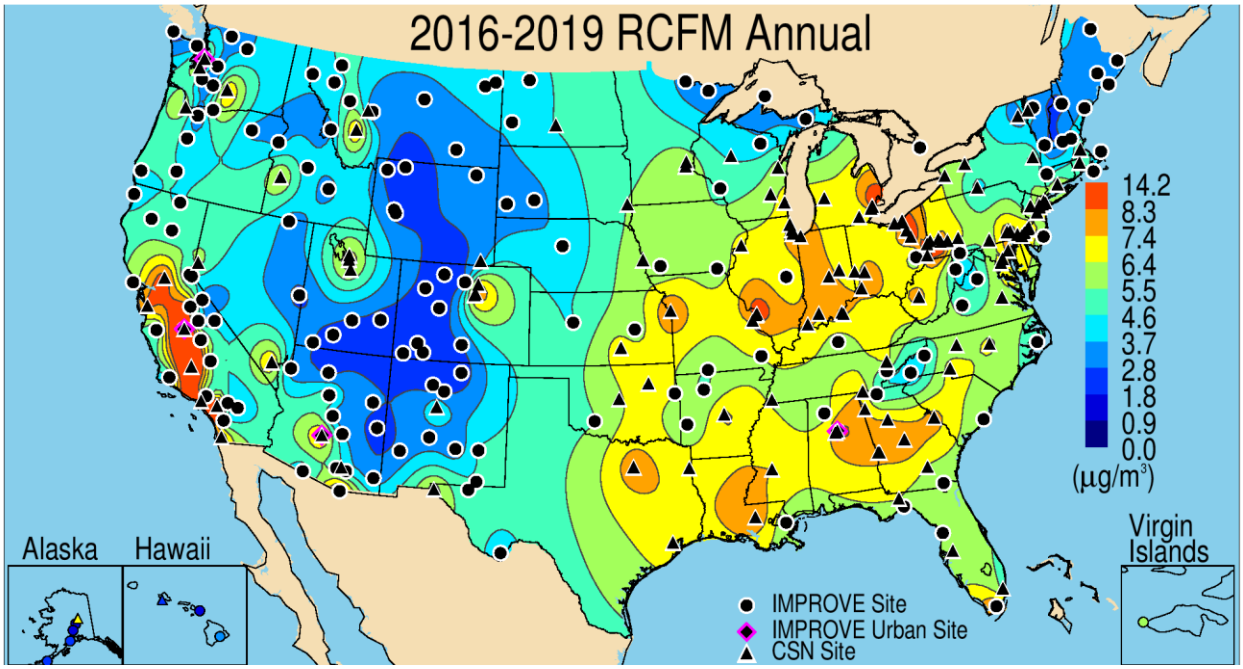

Figure 2.2.9b. IMPROVE and CSN 2016–2019 $PM_{2.5}$ annual mean reconstructed fine mass (RCFM) concentrations (µg m^{-3}).

2.2.10 $PM_{2.5}$ Residual

The residual in fine mass (FM - RCFM) was computed to investigate the level of agreement between RCFM and measured FM concentrations. Differences may be related to the sampling artifacts associated with FM as discussed earlier, such as loss of volatile species or retained water on the filter. Biases could be related to inappropriate molecular forms of assumed species applied in the RCFM algorithm. For example, sulfate could be in a more acidic form, nitrate could be associated with coarse mode species, and OM/OC ratios used to derive POM could be inappropriate, as could the FD algorithm. A detailed investigation into biases associated with FM measurements is presented in Appendix 2.1 and by Hand et al. (2019b). The results from this study informed the changes in the RCFM algorithm included in Table 2.1, specifically regarding calculations of POM and FD.

The residual for most of the rural IMPROVE sites (Figure 2.2.10a) ranged from -3.27 µg m^{-3} at Everglades NP, Florida (EVER1), to 0.78 µg m^{-3} at Point Reyes NP, California (PORE1). The estimated uncertainty in the residual is 0.1 µg m^{-3} (Hand et al., 2019b) based on uncertainty estimates reported in Hyslop and White (2008). The highest annual mean residuals that occurred at sites in the eastern United States may be associated with particle bound water on filters laden with AS (Hand et al., 2019b). Some of the most-negative residuals occurred in the Northwest regions that were influenced by biomass smoke during this period. It is possible that the OM/OC ratio used to compute POM were too low for the smoke conditions at these sites. Negative residuals at sites in southern and central California may also be associated with losses of nitrate from the Teflon filters used to measure gravimetric mass.

Interpretation of the residual for CSN has the added complication of different samplers used to collect filters for gravimetric weighing and for speciated analyses, which could introduce

additional sampling biases and contribute to larger residuals. The annual mean residual at CSN sites ranged from -2.05 μg m^{-3} at Five Points, Ohio (391530023), to 1.78 μg m^{-3} at Parr, Arkansas (051190007). The general spatial pattern in the annual mean residual of the combined IMPROVE-CSN data was similar to IMPROVE-only, with higher residuals at sites in the East and lower residuals at sites in the West (Figure 2.2.10b). Urban sites in the West associated with positive residuals corresponded to Salt Lake City, Utah; Butte, Montana; and Yakima, Washington.

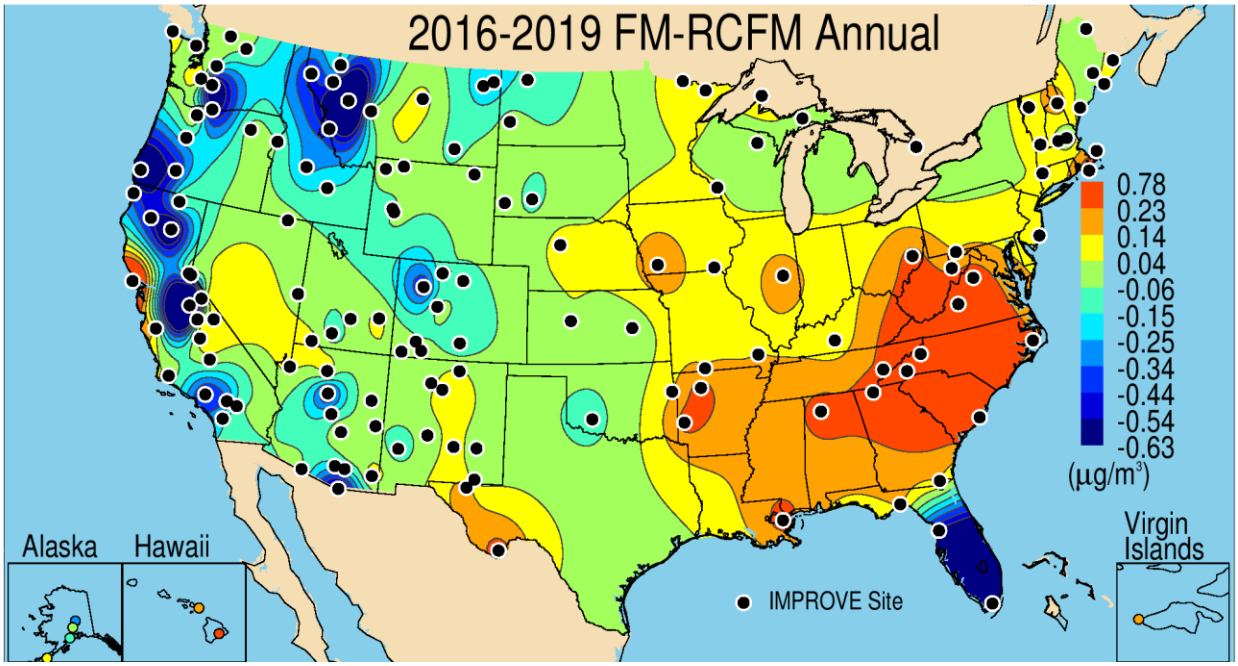

Figure 2.2.10a. IMPROVE 2016–2019 annual mean $PM_{2.5}$ residuals (FM - RCFM) between $PM_{2.5}$ gravimetric fine mass (FM) and reconstructed fine mass (RCFM) (μg m^{-3}).

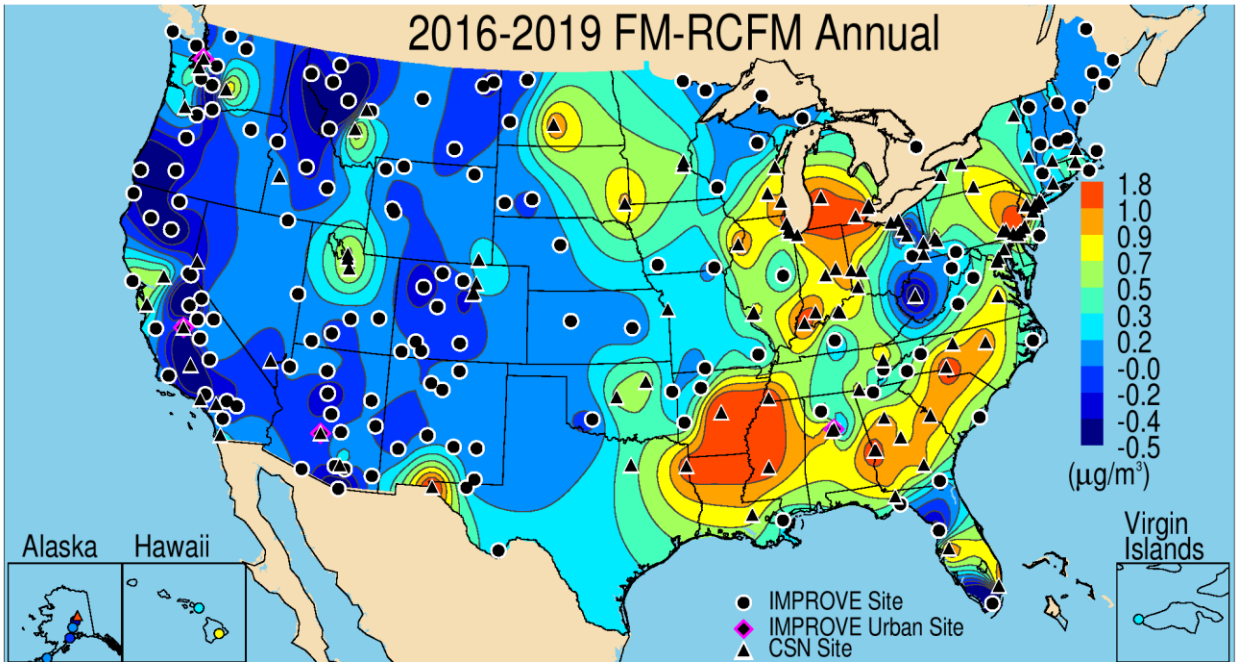

Figure 2.2.10b. IMPROVE and CSN 2016–2019 annual mean $PM_{2.5}$ residuals (FM - RCFM) between $PM_{2.5}$ gravimetric fine mass (FM) and reconstructed fine mass (RCFM) (μg m^{-3}).

2.2.11 PM_{10} Mass

PM_{10} concentrations are not routinely measured at CSN sites; therefore EPA's FRM PM_{10} samplers were used for urban PM_{10} concentrations. These data are reported at standard pressure and temperature (STP) and therefore were adjusted to local conditions for comparison with IMPROVE PM_{10} data (see Hand et al., 2019b). Completeness criteria were applied following the description given above for speciated data, resulting in 399 PM_{10} sites. PM_{10} concentrations include contributions from $PM_{2.5}$ species, in addition to contributions from coarse mode species. Therefore, spatial patterns may be similar to the $PM_{2.5}$ concentrations depending on location and sources but may differ in locations where coarse mode contributions are significant.

The spatial pattern of 2016–2019 IMPROVE annual mean PM_{10} mass concentrations are shown in Figure 2.2.11a. The highest annual mean concentrations occurred at sites in the central United States, along the southwest border with Mexico, and the Central Valley of California. The highest IMPROVE annual mean PM_{10} concentration occurred at Nogales, Arizona (28.68 μg m^{-3}, NOGA1), and the second highest PM_{10} concentration occurred at Virgin Islands NP (18.68 μg m^{-3}, VIIS1), likely due to high SS and FD contributions. The lowest annual mean IMPROVE PM_{10} concentration occurred at Haleakala Crater NP, Hawaii (1.15 μg m^{-3}, HACR1). The spatial pattern of rural PM_{10} concentrations generally followed the patterns of $PM_{2.5}$ concentrations, with higher values at sites in the eastern half of the United States, relatively low values at sites in the Intermountain/Southwest and Northwest, and increased values at sites in California. However, there are some important differences. Sites in the central United States had high PM_{10} concentrations, suggesting additional coarse mass contributions in that region.

The combined IMPROVE and EPA PM_{10} mass concentrations (Figure 2.2.11b) demonstrated higher spatial variability compared to the IMPROVE-only map, in part because of the higher EPA PM_{10} site density. An overall similar pattern existed, with higher PM_{10} concentrations at sites in the central United States, lower concentrations at sites in the Intermountain/Southwest and Northwest, and higher concentrations at sites along the U.S–Mexico border and the Central Valley of California. Additional hot spots of high annual mean PM_{10} concentrations also occurred near Denver, Colorado; El Paso, Texas; Mission and Edinburg, Texas; St. Louis, Missouri; and Minneapolis, Minnesota. The PM_{10} concentrations were also much higher at the EPA sites, suggesting local sources. The urban PM_{10} annual mean concentrations ranged from 3.04 μg m^{-3} at Cornwall, Connecticut (090050005), to 49.50 μg m^{-3} in Bakersfield, California (060290010).

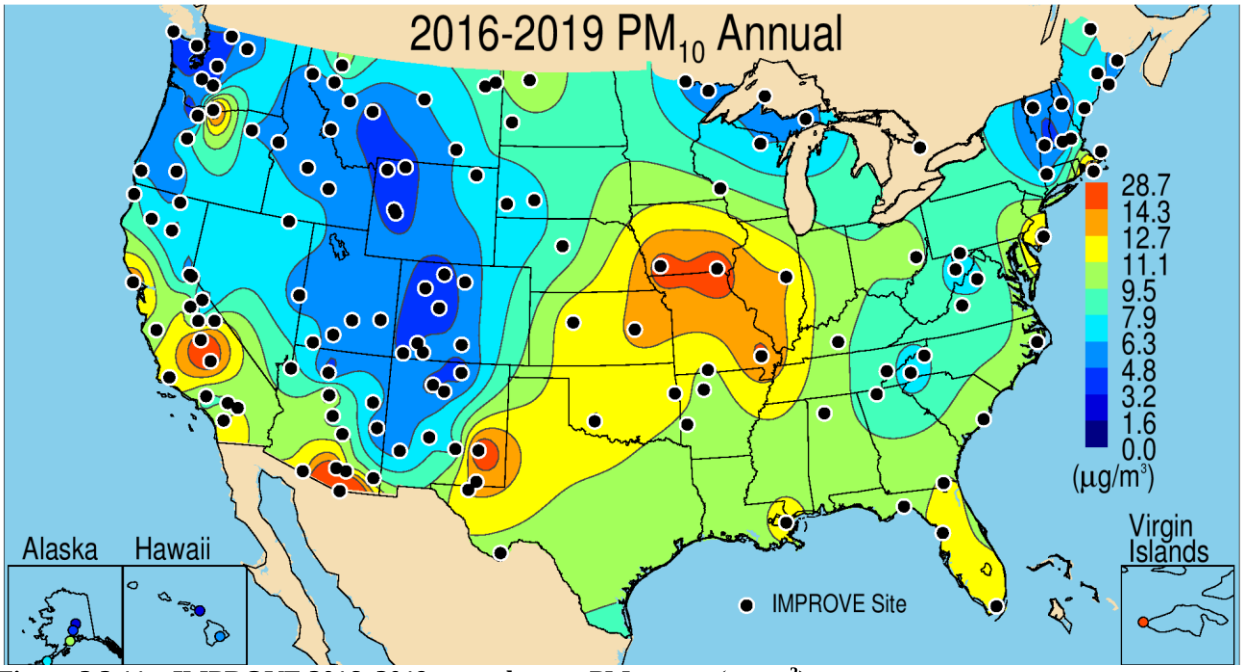

Figure 2.2.11a. IMPROVE 2016–2019 annual mean PM_{10} mass (µg m^{-3}).

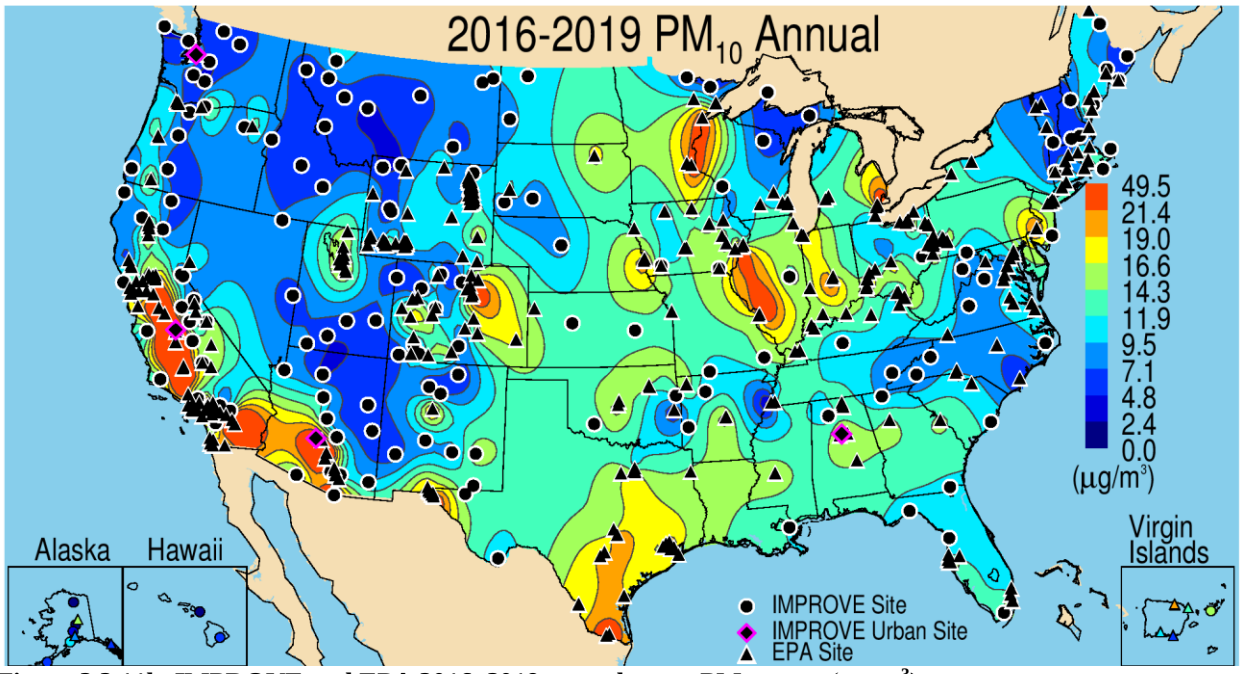

Figure 2.2.11b. IMPROVE and EPA 2016–2019 annual mean PM_{10} mass (µg m^{-3}).

2.2.12 Coarse Mass

CM concentrations are calculated as the difference between gravimetric PM_{10} and $PM_{2.5}$ mass concentrations (PM_{10} - $PM_{2.5}$). Since PM_{10} filters are not routinely analyzed for speciation, CM concentrations are also not speciated. CM concentrations were calculated at IMPROVE sites and at collocated urban/suburban EPA FRM $PM_{2.5}$ (not just CSN locations) and PM_{10} sites, resulting in 198 EPA sites. CM is often assumed to be associated with mineral dust, although

other studies have shown it also could include ionic species such as sodium or nitrate, or organic carbon (e.g., Malm et al., 2007; Lee et al., 2008; Allen et al., 2015; Bondy et al., 2018; Hand et al., 2019b), with sources such as sea salt or biological particles.

The 2016–2019 annual mean rural CM concentrations ranged from 0.97 μg m^{-3} in Haleakala Crater NP, Hawaii (HACR1), to 20.09 μg m^{-3} in Nogales, Arizona (NOGA1) (Figure 2.2.12a), where the highest annual mean FD concentrations also occurred. The second-highest CM occurred at the Virgin Islands NP (13.12 μg m^{-3}, VIIS1). The spatial patterns of CM in the Southwest were similar to those of FD and suggest similar sources (Hand et al., 2017). Higher concentrations also occurred at sites in the California's Central Valley. At sites in the central United States, higher concentrations most likely corresponded to agricultural activity and fugitive dust sources (Hand et al., 2019a; Lambert et al., 2020). Lower annual mean CM concentrations occurred at sites across the Intermountain West, the Northwest, and along the eastern United States into the Northeast.

The overall spatial patterns in urban annual mean CM concentrations (Figure 2.2.12b) were similar to those at rural sites, with higher values at sites in the central United States and along the U.S.–Mexico border and California's Central Valley. Hot spots of CM concentrations were similar to hot spots in PM_{10} concentrations, such as at Salt Lake City, Utah; Denver, Colorado; and St. Louis, Missouri. The highest annual mean urban CM concentration (34.76 μg m^{-3}) occurred at Bakersfield, California (060290010) and the lowest annual mean CM concentration (0.51 μg m^{-3}) occurred at Castle Hayne, North Carolina (371290002), near Wilmington.

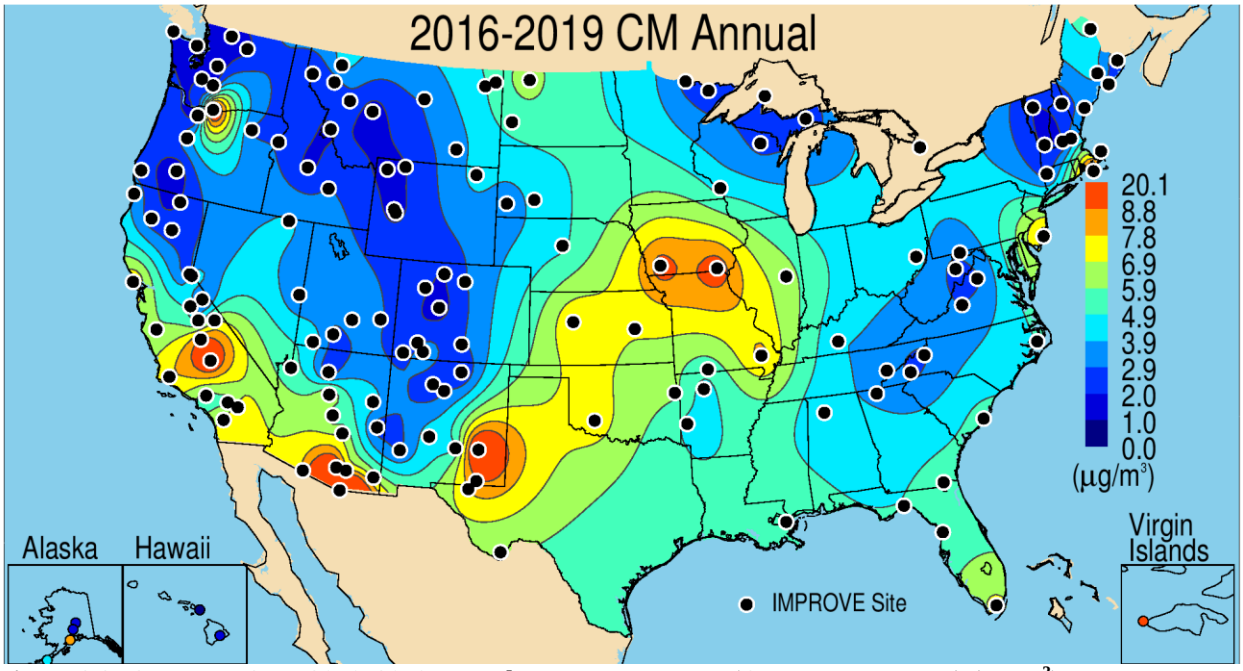

Figure 2.2.12a. IMPROVE 2016–2019 annual mean coarse mass (CM = PM_{10} - $PM_{2.5}$) (μg m^{-3}).

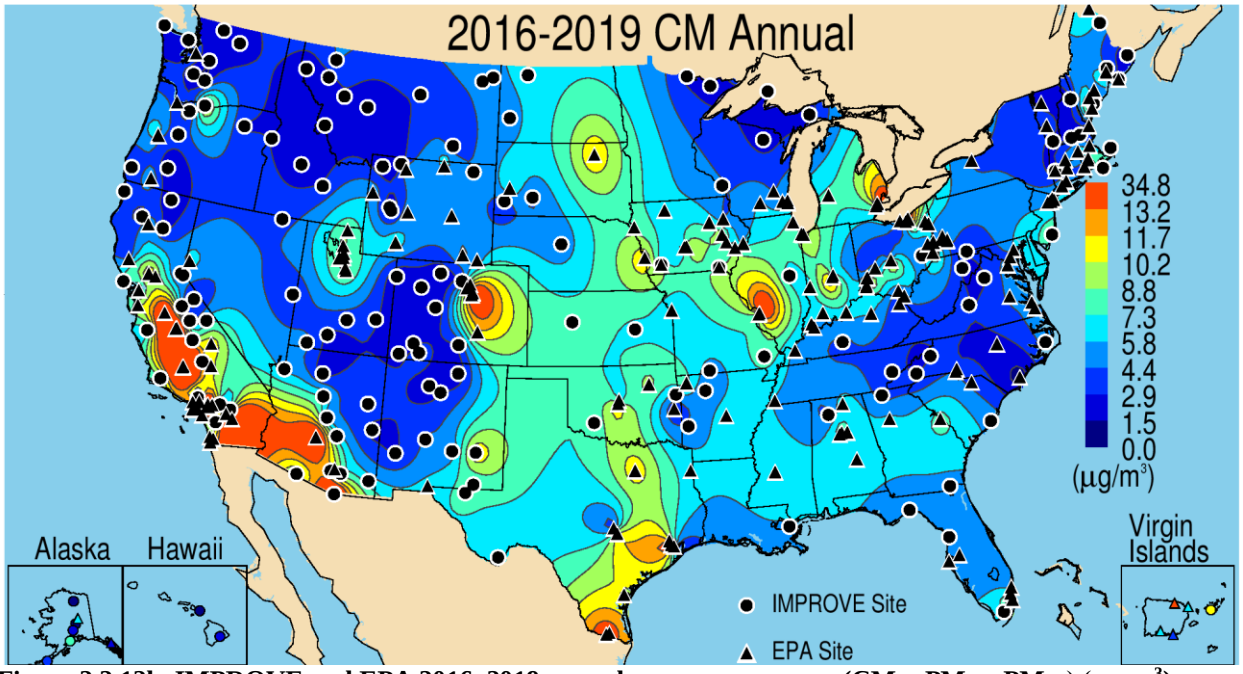

Figure 2.2.12b. IMPROVE and EPA 2016–2019 annual mean coarse mass (CM = PM_{10} - $PM_{2.5}$) (µg m^{-3}).

The fractional contribution of annual mean CM to PM_{10} (CM/PM_{10}) shown in Figure 2.2.12c demonstrated the importance of CM to PM_{10} concentrations at rural sites, especially at sites in the central and southwestern United States. Over half of annual mean PM_{10} concentrations were due to CM for most of the sites in the central United States and for sites in portions of the Intermountain West. Sites in the Southwest had higher contributions, ranging from ~0.6 to 0.8. Contributions were lower at sites in the East and Northwest, with values around 0.3 to 0.4. The highest rural CM fraction (0.83) occurred at Kenai Peninsula Borough, Alaska (KPBO1), and the lowest contribution (0.2) occurred at Crater Lake NP, Oregon (CRLA1).

At urban EPA sites, the spatial variability of annual mean CM/PM_{10} was very similar to rural sites, with higher values at sites in the central United States and Southwest (Figure 2.2.12d). The addition of urban sites provided more spatial detail, especially in the East. The lowest annual mean contribution (0.18) occurred at Castle Hayne, North Carolina (371290002), near Wilmington, similar to the lowest annual mean urban CM concentration. The largest contribution (0.78) occurred at Indio, California (060652002), near the Salton Sea.

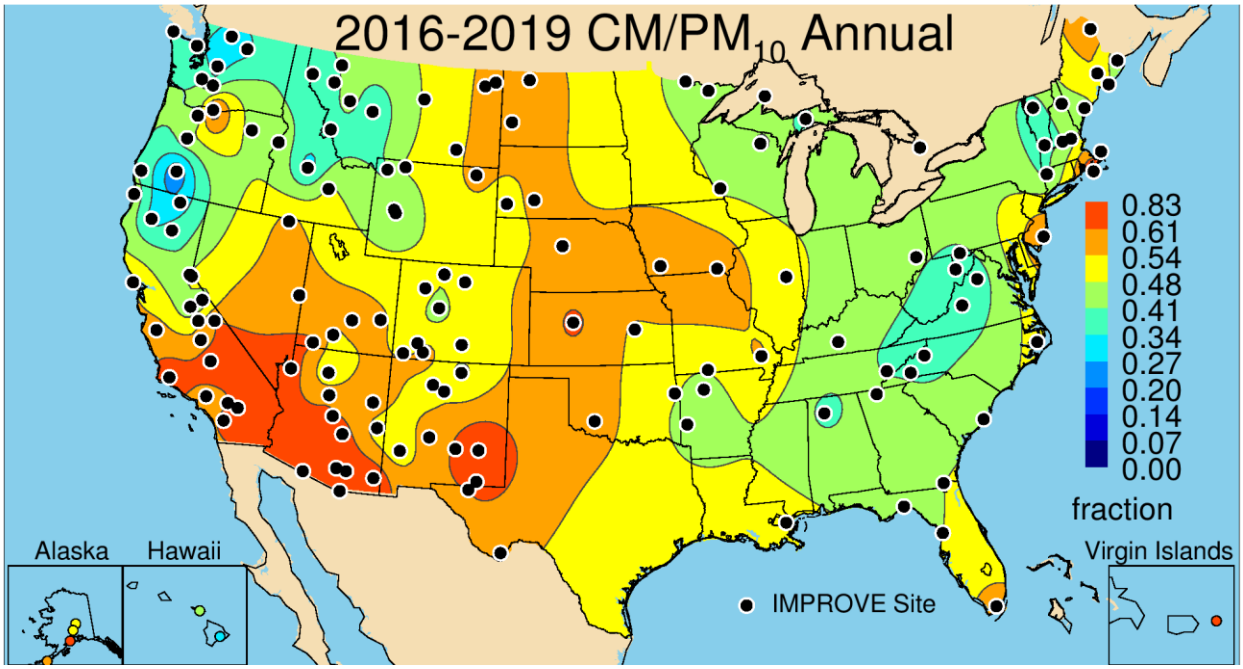

Figure 2.2.12c. IMPROVE 2016–2019 annual mean fraction contributions of CM to PM_{10} gravimetric mass.

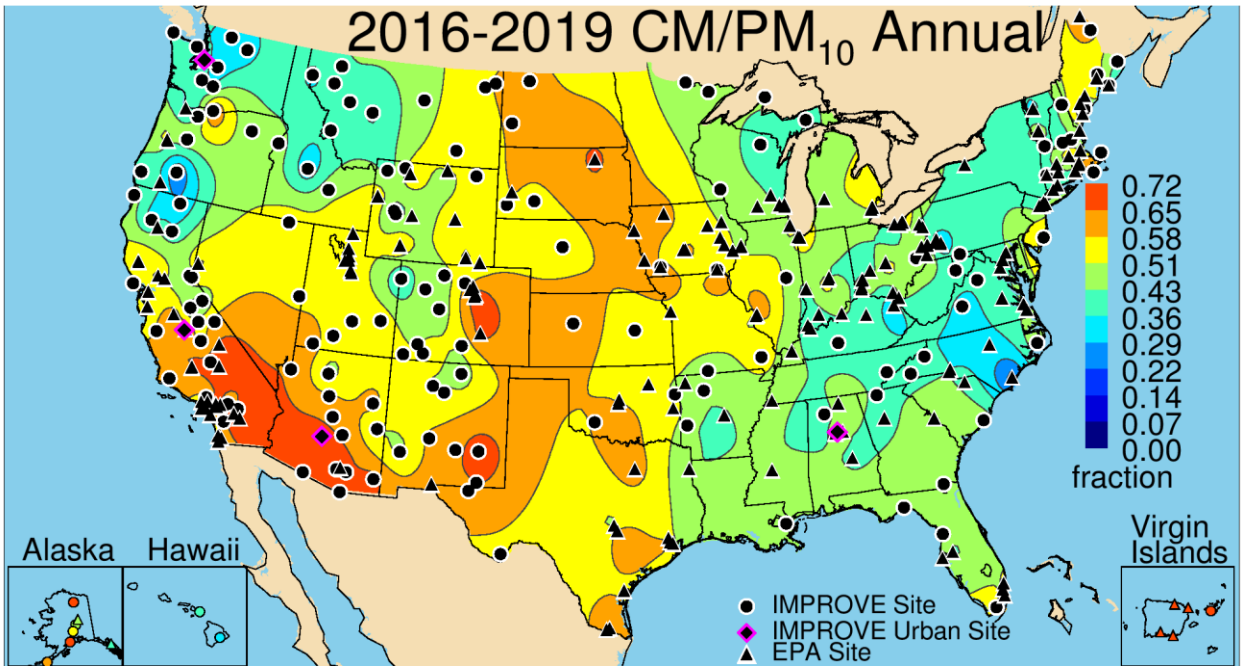

Figure 2.2.12d. IMPROVE and EPA 2016–2019 annual mean fraction contributions of CM to PM_{10} gravimetric mass.

2.2.13 Summary

The spatial variability of FM depends on sources, sinks, and transport of speciated aerosols. A strong spatial gradient in FM was observed, with higher concentrations at sites in the eastern United States. FM decreased rapidly moving westward, with concentrations that were half of those at sites in the East, especially for sites in the Intermountain West. Higher concentrations occurred at sites in California and sites in Oregon and Washington. The spatial

patterns did not change significantly with the addition of urban sites, although urban concentrations were higher, including several hot spots at sites in the West, and at sites in the Central Valley of California. The lowest concentrations of annual mean FM occurred at sites in the Intermountain West and Southwest and at sites in the Northeast. FM and PM_{10} had similar spatial variability, except that rural PM_{10} concentrations were highest at sites in the central United States, rather than for sites throughout the East. The addition of urban PM_{10} sites suggested additional urban sources, with much higher annual mean PM_{10} concentrations at sites in the central United States, southern Arizona, southern Texas, the Front Range of Colorado, southern California, and the Central Valley of California.

The spatial patterns of FM reflected the combined patterns of AS, AN, and POM. AS concentrations were highest in the eastern United States, where SO_2 emissions were highest, and AS contributed significantly to FM in those regions (~0.3). Rural AN concentrations were highest at sites in the central United States and contributed to high FM at sites in that region (0.2–0.3). Additional urban sources influenced urban FM sites at regions in the Central Valley of California, as well as other urban hot spots in the West.

Rural POM concentrations were highest at sites in the northwestern United States, where biomass smoke impacts influenced concentrations, and at sites in the eastern United States, due to biogenic emissions and biomass smoke. The lowest annual mean POM concentrations occurred at sites in the Intermountain West and Southwest. The general spatial patterns of urban and rural POM concentration were similar to rural-only patterns, although higher urban concentrations occurred at sites in Southeast and Central Valley. Contributions of POM to RCFM were significant at sites in the western United States, around 0.7 or greater, and this fraction was similar for CSN sites. At sites in the eastern United States, contributions at CSN sites was around 0.6 or greater, while for rural sites it was around 0.5. Annual mean EC concentrations followed similar patterns to those of POM concentrations at rural sites, with higher concentrations at sites both in the eastern and western United States. Urban EC concentrations were considerably higher than at rural sites, indicating the importance of localized urban sources. Contributions of EC to RCFM at urban sites were roughly double relative to at rural sites (~0.1 relative to ~0.05). Filter light absorption (f_{abs}) was also higher at sites with elevated EC concentrations, suggesting that most of the $PM_{2.5}$ absorption was due to EC, although it was somewhat elevated at sites in the Southwest, perhaps due to the role of iron absorption in dust.

The spatial pattern of FD mass reflected its source areas, with high concentrations at both rural and urban sites in the Southwest, where local and regional sources affect FD concentrations. Sites in the Central Valley also had high FD concentrations, especially for urban sites. Higher annual mean FD at sites in the Southeast reflected the influence of North African dust transport to that area, both for rural and urban sites. FD contributions to RCFM at sites in the Southwest were over 0.5 for many sites in the region. The spatial variability in annual mean CM was similar to FD, especially for sites in the Southwest, suggesting similar sources. However, higher annual mean CM at sites in the central United States, relative to FD patterns, suggested additional sources of coarse-mode aerosol or larger size distributions of dust relative to sources in the Southwest. Urban sites with high CM concentrations occurred in the Central Valley and southern Arizona. CM contributed significantly to PM_{10}, especially at sites in the western United States, where annual mean contributions were over 0.6. For sites in the eastern

United States, the contribution of CM to PM_{10} was ~0.3–0.4. Similar contributions occurred for sites in the Northwest.

SS concentrations, while likely underestimated, also followed suspected marine sources, with higher values along coastal areas for both IMPROVE and CSN sites. SS contributions could be significant (>0.1) at some sites, especially in Alaska and Hawaii, and along the coasts.

The spatial pattern in the annual mean fine mass residuals indicated potential biases associated with the measurements or reconstruction algorithms. Positive residuals at sites in the eastern United States were likely associated with the influence of particle bound water on gravimetric mass measurements from hygroscopic species. In the northwestern United States, sites with negative residuals likely reflected the impact of biomass burning on POM, indicating that the assumed OM/OC ratio may have been too low to account for the wildfire smoke sources of POM.

Tables listing 2016–2019 annual mean concentrations for each site for the IMPROVE network and the CSN are provided in Appendix 2.2. Annual mean $PM_{2.5}$ mass fractions are listed according to site for the IMPROVE network and the CSN in Appendix 2.3.

REFERENCES

Aiken, A. C., Decarlo, P. F., Kroll, J. H., Worsnop, D. R., Huffman, J. A., Docherty, K. S., Ulbrich, I. M., Mohr, C., Kimmel, J. R., and Sueper, D. (2008), O/C and OM/OC ratios of primary, secondary, and ambient organic aerosols with high-resolution time-of-flight aerosol mass spectrometry, *Environmental Science & Technology*, *42*(12), 4478-4485, doi:10.1021/es703009q.

Allen, H. M., Draper, D. C., Ayres, B. R., Ault, A., Bondy, A., Takahama, S., Modini, R. L., Baumann, K., Edgerton, E., Knote, C., Laskin, A., Wang, B., and Fry, J. L. (2015), Influence of crustal dust and sea spray supermicron particle concentrations and acidity on inorganic NO3- aerosol during the 2013 Southern Oxidant and Aerosol Study, *Atmospheric Chemistry and Physics*, *15*(18), 10669-10685, doi:10.5194/acp-15-10669-2015.

Bae, M.-S., Demerjian, K. L., and Schwab, J. J. (2006), Seasonal estimation of organic mass to organic carbon in PM2. 5 at rural and urban locations in New York state, *Atmospheric Environment*, *40*(39), 7467-7479, https://doi.org/10.1016/j.atmosenv.2006.07.008.

Blanchard, C., Hidy, G., Shaw, S., Baumann, K., and Edgerton, E. (2016), Effects of emission reductions on organic aerosol in the southeastern United States, *Atmospheric Chemistry and Physics*, *16*(1), 215-238, doi:10.5194/acp-16-215-2016.

Bond, T. C., Doherty, S. J., Fahey, D. W., Forster, P. M., Berntsen, T., DeAngelo, B. J., Flanner, M. G., Ghan, S., Kärcher, B., and Koch, D. (2013), Bounding the role of black carbon in the climate system: A scientific assessment, *Journal of Geophysical Research: Atmospheres*, *118*(11), 5380-5552, doi:10.1002/jgrd.50171.

Bondy, A. L., Bonanno, D., Moffet, R. C., Wang, B., Laskin, A., and Ault, A. P. (2018), The diverse chemical mixing state of aerosol particles in the southeastern United States, *Atmospheric Chemistry and Physics*, *18*(16), 12595-12612, doi:10.5194/acp-18-12595-2018.

Bozlaker, A., Prospero, J. M., Price, J., and Chellam, S. (2019), Identifying and quantifying the impacts of advected North African dust on the concentration and composition of airborne fine particulate matter in Houston and Galveston, Texas, *Journal of Geophysical Research: Atmospheres*, *124*(22), 12282-12300, doi:https://doi.org/10.1029/2019JD030792.

Chen, Y., Shen, H., and Russell, A. G. (2019), Current and future responses of aerosol ph and composition in the US to declining SO2 emissions and increasing NH3 emissions, *Environmental Science & Technology*, *53*(16), 9646-9655, doi:10.1021/acs.est.9b02005.

Chow, J. C., Watson, J. G., Lowenthal, D. H., and Magliano, K. L. (2005), Loss of PM2.5 nitrate from filter samples in central California, *Journal of the Air & Waste Management Association*, *55*(8), 1158-1168, doi:10.1080/10473289.2005.10464704.

Chow, J., Watson, J., Chen, L.-W., Rice, J., and Frank, N. (2010), Quantification of PM 2.5 organic carbon sampling artifacts in US networks, *Atmospheric Chemistry and Physics*, *10*(12), 5223-5239, doi:https://doi.org/10.5194/acp-10-5223-2010.

Creamean, J. M., Spackman, J. R., Davis, S. M., and White, A. B. (2014), Climatology of long-range transported Asian dust along the West Coast of the United States, *Journal of Geophysical Research: Atmospheres*, *119*(21), 12,171-112,185, doi:10.1002/2014JD021694.

Debell, L. J., Gebhart, K., Hand, J. L., Malm, W. C., Pitchford, M. L., Schichtel, B. S., and White, W. H. (2006), IMPROVE (Interagency Monitoring of Protected Visual Environments): Spatial and seasonal patterns and temporal variability of haze and its constituents in the United States: Report IV, Colorado State University, Fort Collins CO, ISSN 0737-5352-74.

El-Zanan, H. S., Lowenthal, D. H., Zielinska, B., Chow, J. C., and Kumar, N. (2005), Determination of the organic aerosol mass to organic carbon ratio in IMPROVE samples, *Chemosphere*, *60*(4), 485-496, doi:10.1016/j.chemosphere.2005.01.005.

El-Zanan, H. S., Zielinska, B., Mazzoleni, L. R., and Hansen, D. A. (2009), Analytical determination of the aerosol organic mass-to-organic carbon ratio, *Journal of the Air & Waste Management Association*, *59*(1), 58-69, doi: 10.3155/1047-3289.59.1.58.

Evanoski-Cole, A., Gebhart, K., Sive, B., Zhou, Y., Capps, S., Day, D., Prenni, A., Schurman, M., Sullivan, A., and Li, Y. (2017), Composition and sources of winter haze in the Bakken oil and gas extraction region, *Atmospheric Environment*, *156*, 77-87, http://dx.doi.org/10.1016/j.atmosenv.2017.02.019.

Frank, N. H. (2006), Retained nitrate, hydrated sulfates, and carbonaceous mass in federal reference method fine particulate matter for six eastern US cities, *Journal of the Air & Waste Management Association*, *56*(4), 500-511, https://doi.org/10.1080/10473289.2006.10464517.

Gebhart, K. A., Day, D. E., Prenni, A. J., Schichtel, B. A., Hand, J. L., and Evanoski-Cole, A. R. (2018), Visibility impacts at Class I areas near the Bakken oil and gas development, *Journal of the Air & Waste Management Association*, *68*(5), 477-493, doi:10.1080/10962247.2018.1429334.

Hallar, A. G., Lowenthal, D. H., Clegg, S. L., Samburova, V., Taylor, N., Mazzoleni, L. R., Zielinska, B. K., Kristensen, T. B., Chirokova, G., and McCubbin, I. B. (2013), Chemical and hygroscopic properties of aerosol organics at Storm Peak Laboratory, *Journal of Geophysical Research: Atmospheres*, *118*(10), 4767-4779, doi:10.1002/jgrd.50373.

Hand, J., Kreidenweis, S., Sherman, D. E., Collett Jr, J., Hering, S., Day, D., and Malm, W. (2002), Aerosol size distributions and visibility estimates during the Big Bend regional aerosol and visibility observational (BRAVO) study, *Atmospheric Environment*, *36*(32), 5043-5055, https://doi.org/10.1016/S1352-2310(02)00568-X.

Hand, J. L., and Malm, W. C. (2006), Review of the IMPROVE equation for estimating ambient light extinction coefficients, Colorado State University, Fort Collins, CO, ISSN 0737-5352-71.

Hand, J. L., Copeland, S., Day, D., Dillner, A., Indresand, H., Malm, W., McDade, C., Moore, C., Pitchford, M., and Schichtel, B. (2011), IMPROVE (Interagency Monitoring of Protected Visual Environments): Spatial and seasonal patterns and temporal variability of haze and its constituents in the United States, Report V, Colorado State University, Fort Collins, CO.

Hand, J. L., White, W., Gebhart, K., Hyslop, N., Gill, T., and Schichtel, B. (2016), Earlier onset of the spring fine dust season in the southwestern United States, *Geophysical Research Letters*, *43*(8), 4001-4009, doi:10.1002/2016GL068519.

Hand, J. L., Gill, T., and Schichtel, B. (2017), Spatial and seasonal variability in fine mineral dust and coarse aerosol mass at remote sites across the United States, *Journal of Geophysical Research: Atmospheres*, *122*(5), 3080-3097, doi:10.1002/2016JD026290.

Hand, J. L., Gill, T. E., and Schichtel, B. A. (2019a), Urban and rural coarse aerosol mass across the United States: Spatial and seasonal variability and long-term trends, *Atmospheric Environment*, *218*, 117025, doi.org/10.1016/j.atmosenv.2019.117025.

Hand, J. L., Prenni, A. J., Schichtel, B. A., Malm, W. C., and Chow, J. C. (2019b), Trends in remote PM2.5 residual mass across the United States: Implications for aerosol mass reconstruction in the IMPROVE network, *Atmospheric Environment*, *203*, 141-152, doi:doi:10.1016/j.atmosenv.2019.01.049.

Hand, J. L., Prenni, A. J., Copeland, S., Schichtel, B. A., and Malm, W. C. (2020), Thirty years of the Clean Air Act Amendments: Impacts on haze in remote regions of the United States (1990–2018), *Atmospheric Environment*, *243*, 117865, https://doi.org/10.1016/j.atmosenv.2020.117865.

Heald, C. L., Collett Jr, J., Lee, T., Benedict, K., Schwandner, F., Li, Y., Clarisse, L., Hurtmans, D., Van Damme, M., and Clerbaux, C. (2012), Atmospheric ammonia and particulate inorganic nitrogen over the United States, *Atmospheric Chemistry and Physics*, *12*, 10295-10312, doi:10.5194/acp-12-10295-2012.

Heald, C. L., and Kroll, J. (2020), The fuel of atmospheric chemistry: Toward a complete description of reactive organic carbon, *Science Advances*, *6*(6), eaay8967, doi:10.1126/sciadv.aay8967.

Hering, S., and Cass, G. (1999), The magnitude of bias in the measurement of PM25 arising from volatilization of particulate nitrate from Teflon filters, *Journal of the Air & Waste Management Association*, *49*(6), 725-733, doi:10.1080/10473289.1999.10463843.

Hidy, G., Blanchard, C., Baumann, K., Edgerton, E., Tanenbaum, S., Shaw, S., Knipping, E., Tombach, I., Jansen, J., and Walters, J. (2014), Chemical climatology of the southeastern United States, 1999–2013, *Atmospheric Chemistry and Physics*, *14*(21), 11893-11914, doi:10.5194/acp-14-11893-2014.

Hu, C., Griffis, T. J., Baker, J. M., Wood, J. D., Millet, D. B., Yu, Z., and Lee, X. (2020), Modeling the sources and transport processes during extreme ammonia episodes in the US corn belt, *Journal of Geophysical Research: Atmospheres*, *125*, e2019JD031207, http://doi.org/10.1029/2019JD031207.

Husar, R. B., Tratt, D., Schichtel, B. A., Falke, S., Li, F., Jaffe, D., Gasso, S., Gill, T., Laulainen, N. S., and Lu, F. (2001), Asian dust events of April 1998, *Journal of Geophysical Research: Atmospheres*, *106*(D16), 18317-18330.

Hyslop, N. P., and White, W. H. (2008), An evaluation of interagency monitoring of protected visual environments (IMPROVE) collocated precision and uncertainty estimates, *Atmospheric Environment*, *42*(11), 2691-2705, doi:10.1016/j.atmosenv.2007.06.053.

Isaaks, E. H., and Mohan Srivastava, R. (1989), *An Introduction to Applied Geostatistics*, Oxford University Press, New York, ISBN 978-0195050134.

Jimenez, J. L., Canagaratna, M., Donahue, N., Prevot, A., Zhang, Q., Kroll, J. H., DeCarlo, P. F., Allan, J. D., Coe, H., and Ng, N. (2009), Evolution of organic aerosols in the atmosphere, S*cience*, *326*(5959), 1525-1529, doi:10.1126/science.1180353.

Kim, P. S., Jacob, D. J., Fisher, J. A., Travis, K., Yu, K., Zhu, L., Yantosca, R. M., Sulprizio, M., Jimenez, J. L., and Campuzano-Jost, P. (2015), Sources, seasonality, and trends of southeast US aerosol: an integrated analysis of surface, aircraft, and satellite observations with the GEOS-Chem chemical transport model, *Atmospheric Chemistry and Physics*, *15*(18), 10411-10433, doi: 10.5194/acp-15-10411-2015.

Kim, D., Chin, M., Cruz, C. A., Tong, D., and Yu, H. (2021), Spring dust in western North America and its interannual variability—understanding the role of local and transported dust, *Journal of Geophysical Research: Atmospheres*, *126*(22), e2021JD035383, https://doi.org/10.1029/2021JD035383.

Lambert, A., Hallar, A. G., Garcia, M., Strong, C., Andrews, E., and Hand, J. L. (2020), Dust impacts of rapid agricultural expansion on the Great Plains, *Geophysical Research Letters*, *47*(20), e2020GL090347, https://doi.org/10.1029/2020GL090347.

Lawal, A. S., Guan, X., Liu, C., Henneman, L. R., Vasilakos, P., Bhogineni, V., Weber, R. J., Nenes, A., and Russell, A. G. (2018), Linked response of aerosol acidity and ammonia to SO2 and NOx emissions reductions in the United States, *Environmental Science & Technology*, *52*(17), 9861-9873, doi: 10.1021/acs.est.8b00711.

Lee, T., Yu, X.-Y., Ayres, B., Kreidenweis, S. M., Malm, W. C., and Collett Jr, J. L. (2008), Observations of fine and coarse particle nitrate at several rural locations in the United States, *Atmospheric Environment*, *42*(11), 2720-2732, doi: 10.1016/j.atmosenv.2007.05.016.

Lowenthal, D., and Kumar, N. (2006), Light scattering from sea-salt aerosols at Interagency Monitoring of Protected Visual Environments (IMPROVE) sites, *Journal of the Air & Waste Management Association*, *56*(5), 636-642, https://doi.org/10.1080/10473289.2006.10464478.

Lowenthal, D., Zielinska, B., Mason, B., Samy, S., Samburova, V., Collins, D., Spencer, C., Taylor, N., Allen, J., and Kumar, N. (2009), Aerosol characterization studies at Great Smoky Mountains National Park, summer 2006, *Journal of Geophysical Research: Atmospheres*, *114*(D8), doi: 10.1029/2008JD011274.

Lowenthal, D., Zielinska, B., Samburova, V., Collins, D., Taylor, N., and Kumar, N. (2015), Evaluation of assumptions for estimating chemical light extinction at US national parks, *Journal of the Air & Waste Management Association*, *65*(3), 249-260, doi:10.1080/10962247.2014.986307.

Malm, W. C., Sisler, J. F., Huffman, D., Eldred, R. A., and Cahill, T. A. (1994), Spatial and seasonal trends in particle concentration and optical extinction in the United States, *Journal of Geophysical Research: Atmospheres*, *99*(D1), 1347-1370, https://doi.org/10.1029/93JD02916.

Malm, W. C., Pitchford, M. L., McDade, C., and Ashbaugh, L. L. (2007), Coarse particle speciation at selected locations in the rural continental United States, *Atmospheric Environment*, *41*(10), 2225-2239, doi:10.1016/j.atmosenv.2006.10.077.

Malm, W. C., Schichtel, B. A., and Pitchford, M. L. (2011), Uncertainties in PM2. 5 gravimetric and speciation measurements and what we can learn from them, *Journal of the Air & Waste Management Association*, *61*(11), 1131-1149, doi: 10.1080/10473289.2011.603998.

Malm, W., Schichtel, B., Hand, J., and Prenni, A. (2020), Implications of organic mass to carbon ratios increasing over time in the rural United States, *Journal of Geophysical Research: Atmospheres*, *125*(5), e2019JD031480.

Moosmüller, H., Chakrabarty, R., and Arnott, W. (2009), Aerosol light absorption and its measurement: A review, *Journal of Quantitative Spectroscopy and Radiative Transfer*, *110*(11), 844-878, doi:10.1016/j.jqsrt.2009.02.035.

Moosmüller, H., Engelbrecht, J. P., Skiba, M., Frey, G., Chakrabarty, R. K., and Arnott, W. P. (2012), Single scattering albedo of fine mineral dust aerosols controlled by iron concentration, *Journal of Geophysical Research: Atmospheres*, *117*(D11), doi:10.1029/2011JD016909.

Murphy, D. M., Froyd, K. D., Bian, H., Brock, C. A., Dibb, J. E., DiGangi, J. P., Diskin, G., Dollner, M., Kupc, A., Scheuer, E. M., Schill, G. P., Weinzierl, B., Williamson, C. J., and Yu, P. (2019), The distribution of sea-salt aerosol in the global troposphere, *Atmos. Chem. Phys.*, *19*(6), 4093-4104, doi:10.5194/acp-19-4093-2019.

Perry, K. D., Cahill, T. A., Eldred, R. A., Dutcher, D. D., and Gill, T. E. (1997), Long-range transport of North African dust to the eastern United States, *Journal of Geophysical Research: Atmospheres*, *102*(D10), 11225-11238, https://doi.org/10.1029/97JD00260.

Philip, S., Martin, R., Pierce, J., Jimenez, J.-L., Zhang, Q., Canagaratna, M., Spracklen, D., Nowlan, C., Lamsal, L., and Cooper, M. (2014), Spatially and seasonally resolved estimate of the ratio of organic mass to organic carbon, *Atmospheric Environment*, *87*, 34-40, http://dx.doi.org/10.1016/j.atmosenv.2013.11.065.

Pitchford, M., Malm, W. C., Schichtel, B. A., Kumar, N., Lowenthal, D., and Hand, J. L. (2007), Revised algorithm for estimating light extinction from IMPROVE particle speciation data, *Journal of the Air & Waste Management Association*, *57*(11), 1326-1336, doi:10.3155/1047-3289.57.11.1326.

Pitchford, M., Poirot, R., Schichtel, B. A., and Malm, W. C. (2009), Characterization of the winter midwestern particulate nitrate bulge, *Journal of the Air & Waste Management Association*, *59*(9), 1061-1069, doi:10.3155/1047-3289.59.9.1061.

Polidori, A., Turpin, B. J., Davidson, C. I., Rodenburg, L. A., and Maimone, F. (2008), Organic PM 2.5: Fractionation by polarity, FTIR spectroscopy, and OM/OC ratio for the Pittsburgh aerosol, *Aerosol Science and Technology*, *42*(3), 233-246, https://doi.org/10.1080/02786820801958767.

Prenni, A., Day, D., Evanoski-Cole, A., Sive, B., Hecobian, A., Zhou, Y., Gebhart, K., Hand, J., Sullivan, A., and Li, Y. (2016), Oil and gas impacts on air quality in federal lands in the Bakken region: an overview of the Bakken Air Quality Study and first results, *Atmospheric Chemistry and Physics*, *16*(3), 1401-1416, doi:10.5194/acp-16-1401-2016.

Prospero, J. M., Ginoux, P., Torres, O., Nicholson, S. E., and Gill, T. E. (2002), Environmental characterization of global sources of atmospheric soil dust identified with the Nimbus 7 Total Ozone Mapping Spectrometer (TOMS) absorbing aerosol product, *Reviews of geophysics*, *40*(1), 2-1-2-31, doi:10.1029/2000RG000095.

Prospero, J. M., Delany, A. C., Delany, A. C., and Carlson, T. N. (2021), The discovery of African dust transport to the Western Hemisphere and the Saharan air layer: A history, *Bulletin of the American Meteorological Society*, *102*(6), E1239-E1260, https://doi.org/10.1175/BAMS-D-19-0309.1.

Pu, B., and Ginoux, P. (2018), Climatic factors contributing to long-term variations in surface fine dust concentration in the United States, *Atmospheric Chemistry and Physics*, *18*(6), 4201-4215, https://doi.org/10.5194/acp-18-4201-2018.

Rivera, N. I. R., Gill, T. E., Gebhart, K. A., Hand, J. L., Bleiweiss, M. P., and Fitzgerald, R. M. (2009), Wind modeling of Chihuahuan Desert dust outbreaks, *Atmospheric Environment*, *43*(2), 347-354, doi:10.1016/j.atmosenv.2008.09.069.

Ruthenburg, T. C., Perlin, P. C., Liu, V., McDade, C. E., and Dillner, A. M. (2014), Determination of organic matter and organic matter to organic carbon ratios by infrared spectroscopy with application to selected sites in the IMPROVE network, *Atmospheric Environment*, *86*, 47-57, http://dx.doi.org/10.1016/j.atmosenv.2013.12.034.

Silvern, R. F., Jacob, D. J., Kim, P. S., Marais, E. A., Turner, J. R., Campuzano-Jost, P., and Jimenez, J. L. (2017), Inconsistency of ammonium–sulfate aerosol ratios with thermodynamic models in the eastern US: a possible role of organic aerosol, *Atmospheric Chemistry and Physics*, *17*(8), 5107-5118, doi:10.5194/acp-17-5107-2017.

Simon, H., Bhave, P., Swall, J., Frank, N., and Malm, W. (2011), Determining the spatial and seasonal variability in OM/OC ratios across the US using multiple regression, *Atmospheric Chemistry and Physics*, *11*(6), 2933-2949, https://doi.org/10.5194/acp-11-2933-2011.

Tong, D., Dan, M., Wang, T., and Lee, P. (2012), Long-term dust climatology in the western United States reconstructed from routine aerosol ground monitoring, *Atmospheric Chemistry and Physics*, *12*(11), 5189-5205, doi:10.5194/acp-12-5189-2012.

Turpin, B. J., and Lim, H.-J. (2001), Species contributions to PM2. 5 mass concentrations: Revisiting common assumptions for estimating organic mass, *Aerosol Science & Technology*, *35*(1), 602-610, doi:10.1080/02786820119445.

Vitousek, P. M., Aber, J. D., Howarth, R. W., Likens, G. E., Matson, P. A., Schindler, D. W., Schlesinger, W. H., and Tilman, D. G. (1997), Human alteration of the global nitrogen cycle: sources and consequences, *Ecological applications*, *7*(3), 737-750, https://doi.org/10.1890/1051-0761(1997)007[0737:HAOTGN]2.0.CO;2.

Warner, J., Dickerson, R., Wei, Z., Strow, L., Wang, Y., and Liang, Q. (2017), Increased atmospheric ammonia over the world's major agricultural areas detected from space, *Geophysical Research Letters*, *44*, 2875-2884, doi:10.1002/2016GL072305.

Watson, J. G., Chow, J. C., Chen, L.-W. A., and Frank, N. H. (2009), Methods to assess carbonaceous aerosol sampling artifacts for IMPROVE and other long-term networks, *Journal of the Air & Waste Management Association*, *59*(8), 898-911,https://doi.org/10.3155/1047-3289.59.8.898.

Weber, R. J., Guo, H., Russell, A. G., and Nenes, A. (2016), High aerosol acidity despite declining atmospheric sulfate concentrations over the past 15 years, *Nature Geoscience*, *9*(4), 282-285, doi:10.1038/NGEO2665.

White, W. H. (2008), Chemical markers for sea salt in IMPROVE aerosol data, *Atmospheric Environment*, *42*(2), 261-274, doi:10.1016/j.atmosenv.2007.09.040.

White, W. H., Trzepla, K., Hyslop, N. P., and Schichtel, B. A. (2016), A critical review of filter transmittance measurements for aerosol light absorption, and de novo calibration for a decade of

monitoring on PTFE membranes, *Aerosol Science and Technology*, *50*(9), 984-1002, http://dx.doi.org/10.1080/02786826.2016.1211615.